NTNU

Norwegian University of
Science and Technology

Advanced Tubing Design

Temperature Modeling

Øystein Lervik

Petroleum Geoscience and Engineering
Submission date: June 2016
Supervisor: Sigbjørn Sangesland, IPT
Co-supervisor: Bjørn Astor Brechan, IPT

Norwegian University of Science and Technology
Department of Petroleum Engineering and Applied Geophysics

Summary

In casing and tubing design, one of the most important aspects is to make the well safe for operation. This includes many complex areas that need thorough understanding, with one being temperature prediction. This is a vital skill to be able to do correctly, especially in high-pressure, high-temperature (HPHT) wells. A great understanding of the mathematics involved is needed to predict wellbore temperatures with high precision.

The mathematics involved in temperature prediction and some of the most important production loads were investigated in this thesis. A model was established in Matlab based on literature on the subject, and the results from the model were compared to results from industry leading software (ILS). A sensitivity analysis of the model was done, by analyzing the sensitivity of some of the parameters.

The effect of neglecting convection from the model was tested. When neglecting convection, there was a high difference in the simulated temperatures. Including the Joule-Thomson effect in the model was also tested. The inclusion showed that for certain values of a correction factor for the Joule-Thomson effect, the simulated fluid temperature were very close to the ILS temperature.

The model can be improved. Implementation of vertical heat transfer into the model, can give a more realistic wellbore heat transfer simulation, and can give more precise predicted temperatures. In addition to this, the results can be compared to data from existing wells, to give less uncertainty from the model.

Sammendrag

Et av de viktigste aspektene i brønndesign er å gjøre brønnen trygg for alle operasjonene som skal bli utført. Dette inneholder mange komplekse tema som behøver grundig forståelse, der et av temaene er temperaturestimering. Temperaturestimering er viktig å gjøre riktig, spesielt i brønner med høyt trykk og høy temperatur. En god forståelse av matematikken bak temperaturestimering er viktig for å få estimeringen så nøyaktig som mulig.

Matematikken bak temperaturestimering og de viktigste lastene som virker i en produksjonsbrønn ble undersøkt i denne masteroppgaven. En modell ble laget i Matlab basert på gjeldende litteratur. Resultatene fra modellen ble sammenlignet med resultat fra programvare som brukes i industrien. En sensitivitesanalyse ble gjennomført ved å analysere sensitiviteten til visse parametere i modellen.

Effekten av å neglisjere konveksjon ble testet. Neglisjeringen førte til store forskjeller i temperaturene. Inkludering av Joule-Thomson-effekten ble også testet. For visse verdier av en korrelasjonsfaktor for Joule-Thomson-effekten, fikk den simulerte temperaturen verdier nær temperaturen fra programvaren fra industrien.

Modellen kan forbedres. Ved å implementere vertikal varmeoverføring i modellen, kan en mer realistisk simulering av varmeoverføring i brønner oppnås. Dette kan igjen gi mer presise verdier for de simulerte temperaturene. I tillegg kan resultatene sammenlignes med data fra ekte brønner for å få mindre usikkerhet i modellen.

Acknowledgements

This thesis is worked out at the Norwegian University of Science and Technology as a final report for TPG4910 – Master's Thesis, Drilling Engineering.

I would like to thank my supervisor Sigbjørn Sangesland for letting me write my thesis as a part of his team, and my co-supervisor Bjørn Brechan for his guidance and expertise. I would also like to thank PhD student Jesus De Andrade for his help with wellbore heat transfer. Lastly, I would like to thank my fellow students here at NTNU for sharing knowledge and ideas.

Table of Contents

List of Figures

List of Tables

Abbreviations

AFE	Annulus Fluid Expansion
APB	Annulus Pressure Build-up
API	American Petroleum Institute
BH	Bottomhole
GOR	Gas/Oil-ratio
HPHT	High-pressure, High-temperature
ILS	Industry Leading Software
MAASP	Maximum Allowable Annular Surface Pressure
MD	Measured Depth
NTNU	Norwegian University of Science and Technology
TOC	Top of Cement
TVD	True Vertical Depth
WH	Wellhead

1 Introduction

Motivation

In tubing and casing design, one of the most important aspects is to make the well safe for operation. Tubing and casing design includes many complex areas that need thorough understanding to ensure as safe operations as possible. Temperature prediction is one of these areas. Especially in HPHT wells, it is a vital skill to be able to predict correct temperatures.

Previous Solutions

There are many papers on the subject, and most temperature prediction literature based on wellbore heat transfer goes back to the paper by Ramey from 1962. He found a method to relate the flowing wellbore fluid to the formation temperatures, which also have been used to calculate wellbore heat loss. During the years with new technology and findings the theory has been improved. Hasan and Kabir have developed a method to effectively predict the flowing wellbore fluid, with high presicion. Knut Vegard Løbergsli made a model for his master's thesis in 2015 which assumed a vertical well with cement in all annuli (Løbergsli, 2015).

Goal

The goal of the thesis is to give a broad understanding of the literature on wellbore heat transfer mechanisms, as well as developing a well functioning model to predict flowing fluid temperatures in Matlab, with a deviated well and with specified cement depths.

Approach

The literature on the subject will be investigated in this thesis, with an explanation of the most important theory. A model will be developed in Matlab to simulate results based on the existing literature. The results will be compared to ILS results. The ILS program used will be WellCat.

2 Theory

2.1 Tubing Stress Analysis

Tubing stress analysis is important in regards to completion design. To get a broad understanding of all the loads acting on the tubing is essential to get the completion design needed to make the tubulars withstand all the loads. Tubing stress analysis is also helping with defining what packers or expansion devices that are required for the well (Bellarby, 2009). Some of the most important loads that are affecting the tubing during production are presented below. Table 2-1 shows the different loads during production, and what type of loads they are, i.e. collapse, burst or axial (Lervik, 2015). The loads that are highlighted in red are not discussed in this thesis.

Table 2-1 Production Loads

	Collapse	**Burst**	**Axial**
Load Case	Pressure Test-Annulus Late-life Production Mid-life Production Tubing Evacuation Tubing Leak	Pressure Test-Tubing Shut-in Early-life-Production Pumping Kill Fluid Bullheading	Temperature Changes Fluid Drag Annulus Pressure Build-up Pumping Kill Fluid Bullheading Tubing Evacuation

2.1.1 Base Case

To get all the loads calculated correctly, it is essential to get the initial conditions, i.e. the base case, correct. These include the initial pressures and temperatures (Bellarby, 2009). A HPHT well is defined as a well that has an expected shut-in pressure that exceeds 69 MPa or that has a static bottomhole pressure higher than 150 °C (NORSOK D-010, 2004).

2.1.2 Pressure Test Tubing

Before the completion is accepted for service, the tubing has to be pressure tested (Bellarby, 2009). This is because the tubing is the primary barrier in most well constructions. The tubing is tested with an applied pressure called “well design pressure”, which is the wellhead pressure plus a margin of 70 bar (NORSOK D-010, 2004).

2.1.3 Pressure Test Annulus

The most important part of pressure testing the annulus is to verify the integrity of the packers or liner hangers. The purpose of pressure testing the A-annulus is to certify the secondary well barrier (NORSOK D-010, 2004).

2.1.4 Production

Production cause thermal changes in the well, and can generate high temperature loads with either high or low pressures in the tubing. Some considerations have to be made for production-related conditions. Firstly, the load case that has the highest temperature must be found from sensitivities to flow rate, pressure and fluids. Secondly, the production loads with high surface pressures are not always examined, because they are included in the shut-in loads. Thirdly, a separate load case is often made for tubing evacuation. If the severity of this load is greater than a low-pressure production load, the tubing evacuation load is deemed too severe, i.e. unlikely to occur, and the low-pressure production load should be examined. Finally, high collapse loads can be produced from a combination of high annulus pressure and high drawdowns. If this collapse load has a possibility to occur, the well design should have a warning for this and the well operation procedures should include the maximum allowable annular surface pressures (MAASP) (Bellarby, 2009).

2.1.5 Shut-in

Both pressures and temperatures can be high during shut-in, so this is a critical load case. Steady-state production with high temperature followed by a quick shut-in is the worst-case scenario for this load, because this generates a combination of high pressure and temperature. The worst-case scenario can often be hard to identify, because the wellhead pressure will rise when the temperature falls (Bellarby, 2009).

2.1.6 Temperature Changes

When metal is heated, it expands. This expansion is given by (Bellarby, 2009):

$$\Delta L_T = C_T \Delta T L \tag{1}$$

Where

$\Delta L_T =$ Metal expansion (ft)

C_T = Coefficient of thermal expansion (°F^{-1})

ΔT = Average change in temperature from base case to load case (°F)

L = Length of tubing (ft)

For tubing that is fixed at both ends, heating will cause compression, while cooling will cause tension. This compressional or tensile force is given by (Bellarby, 2009):

$$F_T = -C_T E \Delta T (A_o - A_i) \quad \textbf{(2)}$$

Where

F_T = Force due to temperature change (lb)

E = Young's modulus (psi)

A_i = Inside area (in^2)

A_o = Outside area (in^2)

When tubulars are heated it is most often caused by production of hotter fluids from depth, while cooling of the tubulars comes from surface injection of colder fluids. Some times injection wells can be hot also, e.g. for gas injectors where the compressors are local to the injection well (Bellarby, 2009).

2.1.7 Fluid Drag

Frictional drag in the tubing occurs when there are fluids flowing through the tubing. This is an axial force and is given by (Bellarby, 2009):

$$F_F = -\frac{\Delta p}{\Delta L} A_i L \quad \textbf{(3)}$$

Where

F_F = Force due to frictional drag (lb)

$\frac{\Delta p}{\Delta L}$ = Friction pressure drop (psi/ft)

When the tubing is free to move, the frictional drag force generates a change in length of the tubing, given by (Bellarby, 2009):

$$\Delta L_F = \frac{-\frac{\Delta p}{\Delta L} L^2 A_i}{2E(A_o - A_i)} \quad \textbf{(4)}$$

Where

$\Delta L_F =$ Length change due to frictional drag (ft)

The forces and length changes that are generated from fluid drag are often small in comparison to forces and length changes from e.g. ballooning, so they are often neglected in software calculations (Bellarby, 2009).

2.1.8 Annulus Pressure Build-up

Thermal expansion of fluids can lead to either an increase in the fluid volume or an increase in the fluid pressure. This is why annulus pressure build-up (APB) or annulus fluid expansion (AFE) is an important issue. Prediction of APB consists of three factors. Firstly, due to an increase in fluid temperature, there is an expansion of fluid. Secondly, ballooning or reverse ballooning of the casing strings lead to changes in containment volume. Finally, fluids removed from the annulus, by bleeding off at surface or leakage of an open shoe (Bellarby, 2009).

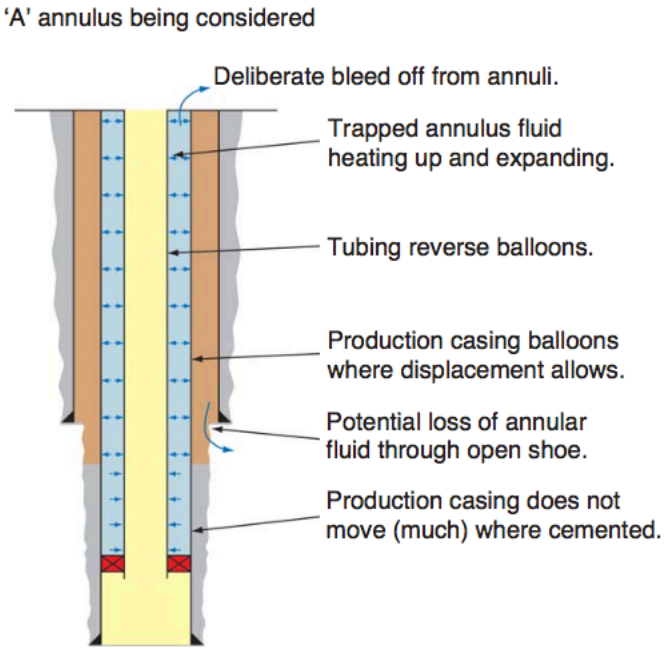

Figure 2-1 Annulus Pressure Build-up (Bellarby, 2009)

The pressure increase resulting from the thermal expansion is given by (Bellarby, 2009):

$$\Delta p = \frac{\alpha \Delta T}{C} \tag{5}$$

Where

$\Delta p =$ Pressure increase due to thermal expansion (psi)

$\alpha =$ Coefficient of thermal expansion of annular fluid ($°F^{-1}$)

$\Delta T =$ Average temperature change in the annulus (°F)

$C =$ Compressibility of the fluid (psi^{-1})

An explanation of more tubing loads can be found in Appendix A.

2.2 Heat Transfer

To understand the concept of heat transfer, an explanation of the terms conduction, convection and radiation is needed. Heat transfer is defined as "thermal energy in transit due to a spatial temperature difference" (Bergman et al., 2011).

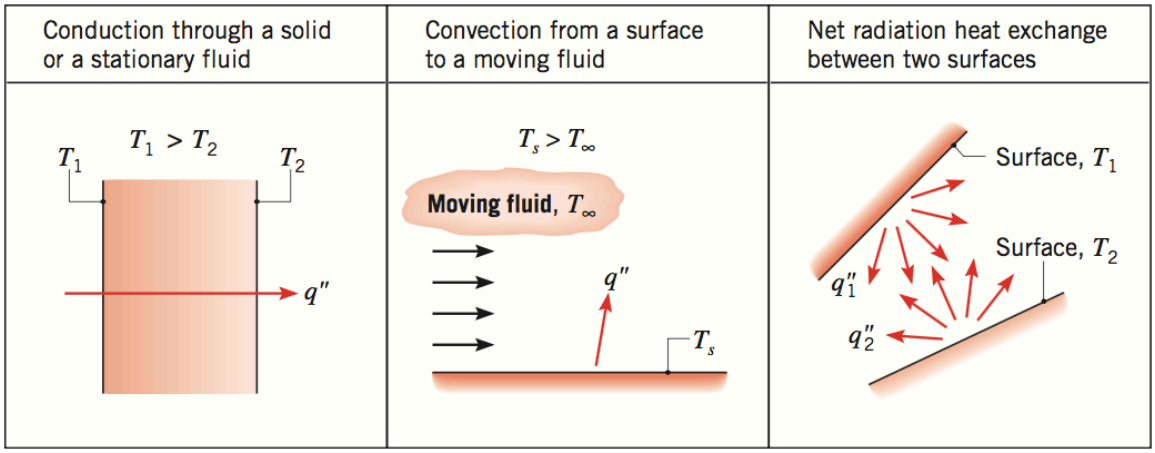

Figure 2-2 Conduction, Convection and Radiation (Bergman et al., 2011)

2.2.1 Conduction

Conduction is referred to as heat transfer that occurs across a stationary medium, in solid or fluid form. Its mechanism is random molecular motion that leads to diffusion of energy (Bergman et al., 2011). Fourier's law governs the equation for convection rate (Bergman et al., 2011):

$$q''_x = -k\frac{dT}{dx} \tag{6}$$

Where

q''_x = Conductive heat transfer rate in x-direction (W/m^2)

k = Thermal conductivity (W/m-K)

$\frac{dT}{dx}$ = Temperature gradient (K/m)

Fourier's law is applicable for both simple and complex conditions. The minus sign comes from the fact that the direction of the heat transfer is with decreasing temperature.

2.2.2 Convection

Convection is referred to as heat transfer that occurs between a moving fluid and a surface that have different temperatures. Its mechanism is as for conduction random molecular motion that leads to diffusion of energy. What makes it differ from conduction is addition of energy transfer due to bulk motion, also called advection (Bergman et al., 2011). The convection rate equation is given as (Bergman et al., 2011):

$$q'' = h(T_s - T_\infty) \quad \textbf{(7)}$$

Where

q'' = Convective heat transfer (W/m^2)

T_s = Surface temperature (K)

T_∞ = Fluid temperature (K)

2.2.3 Radiation

Radiation is referred to as heat transfer between two surfaces with different temperatures, in the form of electromagnetic waves. The radiation is energy that is emitted from matter at a nonzero temperature. Radiation does not need the presence of a material medium (Bergman et al., 2011). The radiation rate is given by (Bergman et al., 2011):

$$q_{rad} = h_r A(T_s - T_{sur}) \quad \textbf{(8)}$$

$$h_r = \varepsilon\sigma(T_s + T_{sur})(T_s^2 + T_{sur}^2) \quad \textbf{(9)}$$

Where

q_{rad} = Radiation heat transfer (W/m^2)

h_r = Radiation heat transfer coefficient (W/m^2-K)

A = Area (m^2)

T_{sur} = Surroundings temperature (K)

ε = Emissivity (dimensionless)

σ = Stefan-Boltzmann constant (=5.67×10^{-8} W/m^2-K^4)

2.3 Temperature Prediction

In tubing stress analysis, temperature prediction of the production or injection fluids and surrounding casing/tubing is a critical skill. Especially in HPHT fields this is critical, to ensure safe and efficient well design. There are several different ways of predicting the temperature in and around the wellbores (Bellarby, 2009).

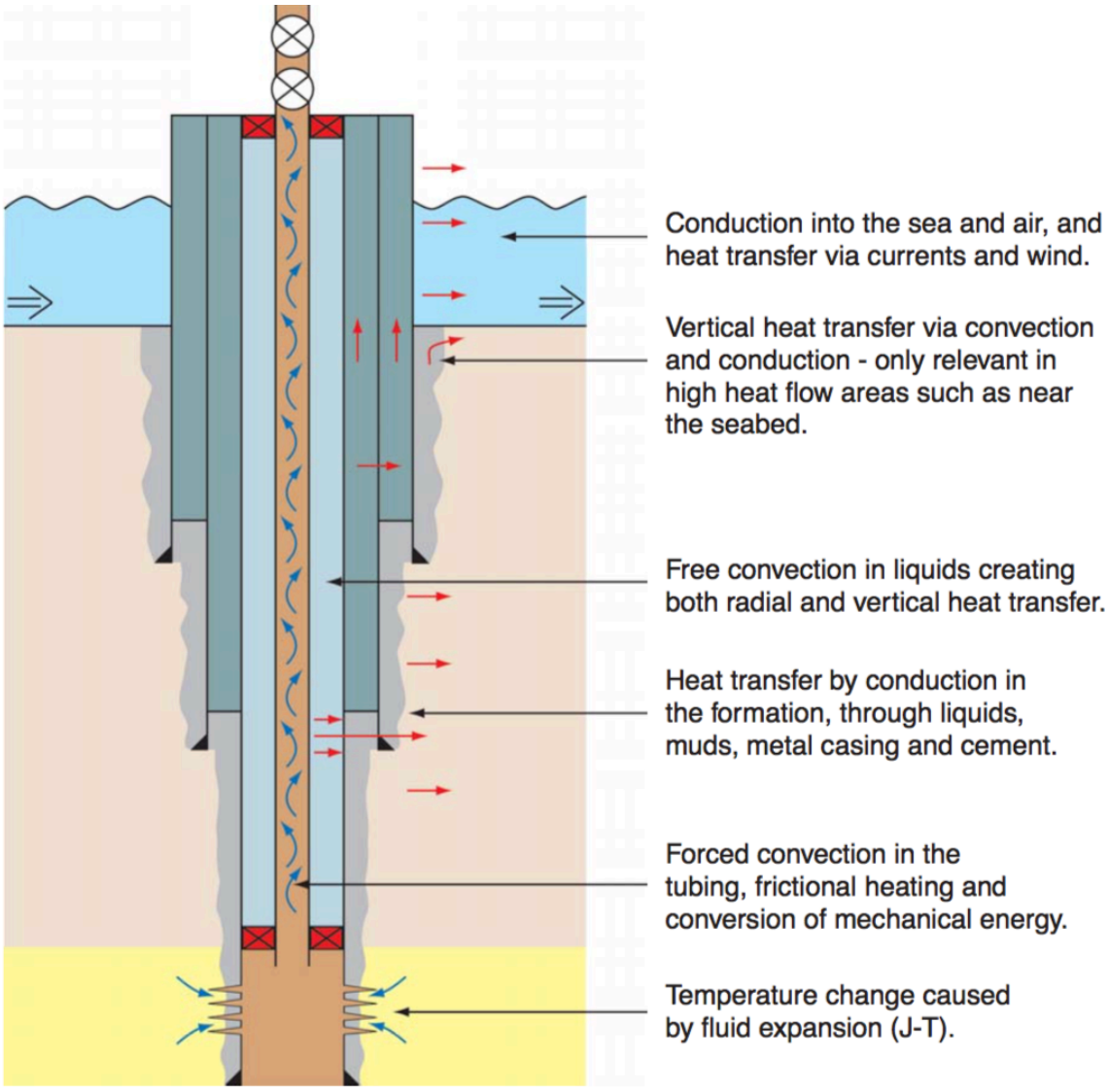

Figure 2-3 Heat Transfer Mechanisms (Bellarby, 2009)

It is of great importance to have an accurate fluid model to obtain accurate temperature predictions. This importance is increased when including phase transfers. For wells that are producing gas, pressure has a great effect on the temperature.

Therefore, when making a prediction model, it is important to iterate on both pressure and temperature. Most prediction models assume constant wellhead flowing pressure and bottomhole flowing temperature (Bellarby, 2009).

Thermal diffusivity governs the heat transfer away from the wellbore. This heat transfer is most often assumed to be radial. The heat transfer is given as (Bellarby, 2009):

$$Q = U\pi D(T_w - T_g) \quad \textbf{(10)}$$

Where

Q = Heat transfer per unit length (Btu/hr)

U = Overall heat transfer coefficient (Btu/hr-ft^2-°F)

D = Diameter of inside completion string (ft)

T_w = Inside tubing temperature (°F)

T_g = Temperature of formation away from wellbore (°F)

The heat transfer coefficient can often be assumed constant, e.g. for steady-state flow. The calculation of this coefficient is dependent on both fluid properties and time (Bellarby, 2009).

2.4 Wellbore Heat Transfer

When fluids move through a wellbore, it causes heat transfer between the fluids and the earth. This heat transfer occurs because of the difference of the fluid and geothermal temperature. Since heat transfer occurs in drilling, production and injection operations, it is important to have great knowledge about this type of heat transmission (Ramey, 1962).

2.4.1 Formation Temperature Distribution

Heat transfer in both the wellbore and the surrounding formation has a diversity of applications to its various aspects. Therefore it is important to have a rigorous approach to the development of applications using heat transfer calculations. A formation temperature distribution can be used with dimensionless temperature and

dimensionless time to allow easy computation of both wellbore heat loss and temperature of flowing fluid for steady-state, two-phase flow (Hasan and Kabir, 1994).

2.4.2 Wellbore Fluid Energy Balance

When a fluid flows up through the wellbore, the heat loss that occurs causes the fluid temperature to decrease. An energy balance for the fluid can be done. For a two-phase system, the following equation can be used (Hasan and Kabir, 1994):

$$\frac{dT_f}{dz} = \frac{1}{c_{pm}} \frac{dH}{dz} + C_J \frac{dp}{dz} \tag{11}$$

$$\frac{dH}{dz} = \frac{dQ}{dz} - \frac{g \sin\theta}{g_c J} - \frac{v}{g_c J} \frac{dv}{dz} \tag{12}$$

Where

T_f = Tubing fluid temperature (°F)

c_{pm} = Wellbore fluid heat capacity (Btu/lbm-°F)

H = Fluid enthalpy (Btu/lbm)

C_J = Joule-Thomson coefficient (dimensionless)

Q = Heat flow rate (Btu/hr)

g = Gravity acceleration (ft/sec^2)

g_c = Conversion factor (=32.2 lbm-ft/lbf-sec^2)

θ = Pipe inclination angle from horizontal (Degrees)

v = Specific volume (ft^3/lbm)

The fluid and the surrounding formation generate a radial heat transfer that can be expressed with an overall heat transfer coefficient, U_{to}. U_{to} is based on the outside surface area of the tubing, and is used in the equation for the heat transfer rate (Hasan and Kabir, 1994) and the component terms of temperatures (Willhite, 1967):

$$\frac{dQ}{dz} = -\frac{2\pi r_{to} U_{to}}{W}(T_f - T_{wb}) \quad \textbf{(13)}$$

$$T_f - T_{wb} = (T_f - T_{ti}) + (T_{ti} - T_{to}) + (T_{to} - T_{ci}) + (T_{ci} - T_{co}) + (T_{co} - T_{wb}) \quad \textbf{(14)}$$

$$U_{to} = [\frac{r_{to}}{r_{ti} h_{to}} + \frac{r_{to}}{r_{ins}(h_c + h_r)} + \frac{r_{to} \ln(\frac{r_{to}}{r_{ti}})}{k_t} + \frac{r_{to} \ln(\frac{r_{ins}}{r_o})}{k_{ins}} + \frac{r_{to} \ln(\frac{r_{co}}{r_{ci}})}{k_{cas}} + \frac{r_{to} \ln(\frac{r_{wb}}{r_{co}})}{k_{cem}}]^{-1} \quad \textbf{(15)}$$

Where

U_{to} = Overall heat transfer coefficient (Btu/hr-ft^2-°F)

W = Total mass flow rate (lbm/sec)

T_f = Tubing fluid temperature (°F)

T_{wb} = Interface temperature wellbore/earth (°F)

T_{ti} = Inside tubing temperature (°F)

T_{to} = Outside tubing temperature (°F)

T_{ci} = Inside casing temperature (°F)

T_{co} = Outside casing temperature (°F)

r_{to} = Tubing outside radius (ft)

r_{ti} = Tubing inside radius (ft)

r_{ins} = Insulation surface radius (ft)

r_{co} = Casing outside radius (ft)

r_{ci} = Casing inside radius (ft)

r_{wb} = Wellbore or cement outside radius (ft)

h_c = Convective heat transfer coefficient for fluid in annulus (Btu/°F-hr-ft^2)

h_r = Radiative heat transfer coefficient for annulus (Btu/°F-hr-ft^2)

k_t = Tubing material conductivity (Btu/hr-ft-°F)

k_{ins} = Insulation material conductivity (Btu/hr-ft-°F)

k_{cas} = Casing material conductivity (Btu/hr-ft-°F)

k_{cem} = Cement conductivity (Btu/hr-ft-°F)

Using the definition for T_D, heat transfer rate can be defined as (Hasan and Kabir, 1994):

$$\frac{dQ}{dz} = -\frac{2\pi k_e}{WT_D}(T_{wb} - T_{ei}) \tag{16}$$

Where

k_e = Earth conductivity (Btu/hr-ft-°F)

T_D = Dimensionless temperature

T_{ei} = Undisturbed formation temperature at any given depth (°F)

By combining equations (13) and (16) the following expression can be obtained for heat transfer rate (Hasan and Kabir, 1994):

$$\frac{dQ}{dz} = -\frac{2\pi}{W}\left(\frac{r_{to}U_{to}k_e}{k_e + T_D r_{to}U_{to}}\right)\left(T_f - T_{ei}\right) \tag{17}$$

2.4.3 Wellbore Fluid Temperature

Wellbore fluid temperature is controlled by the heat loss rate going from the wellbore to the formation surrounding it. This rate is varying with depth and the production or injection time. To define an equation for wellbore fluid temperature varying with depth, heat transfer rate is eliminated from equations (11) and (17). Wellbore fluid temperature is therefore defined as (Hasan and Kabir, 1994):

$$\frac{dT_f}{dz} = \frac{T_{ei} - T_f}{A} - \frac{g}{g_c}\frac{\sin\theta}{Jc_{pm}} + C_J\frac{dp}{dz} - \frac{vdv}{g_c Jc_{pm}} \tag{18}$$

$$A = \frac{c_{pm}W}{2\pi}\left(\frac{k_e + r_{to}U_{to}T_D}{r_{to}U_{to}k_e}\right) \tag{19}$$

$$T_{ei} = T_{eibh} - g_T z \tag{20}$$

Where

$A =$ Inverse relaxation distance (ft)

$T_{eibh} =$ Undisturbed bottomhole formation temperature (°F)

$g_T =$ Geothermal temperature gradient (°F/ft)

$z =$ Depth from surface (ft)

For a producing well with known fluid and formation temperatures at bottomhole conditions, the following expression for fluid temperature varying with well depth is obtained (Hasan and Kabir, 1994):

$$T_f = T_{ei} + A\left[1 - e^{(z_{bh}-z)/A}\right]\left(-\frac{g\sin\theta}{g_c J c_{pm}} + \phi + g_T \sin\theta\right) + e^{(z_{bh}-z)/A}\left(T_{fbh} - T_{ebh}\right) \tag{21}$$

$$\phi = -2.978\times10^{-3} + 1.006\times10^{-6} p_{wh} + 1.906\times10^{-4} w_t - 1.047\times10^{-6} R_{gL} + 3.229\times10^{-5}\gamma_{API} + 4.009\times10^{-3}\gamma_g - 0.3551 g_G \tag{22}$$

Where

$z_{bh} =$ Total depth from surface (ft)

$\phi =$ Correction factor including the Joule-Thomson effect for each length interval in the well (dimensionless)

$T_{fbh} =$ Bottomhole fluid temperature (°F)

$T_{ebh} =$ Bottomhole formation temperature (°F)

$p_{wh} =$ Wellhead pressure (psi)

$w_t =$ Total mass flow rate (lbm/sec)

$R_{gL} =$ °Gas/liquid ratio (scf/STB)

$\gamma_{API} =$ Oil gravity (°API)

$\gamma_g =$ Gas specific gravity

$g_G =$ Geothermal gradient (°F/ft)

The equation for ϕ is applicable for $w_t < 5$ lbm/sec, while ϕ=0 for $w_t \geq 5$ lbm/sec (Sagar et al., 1991).

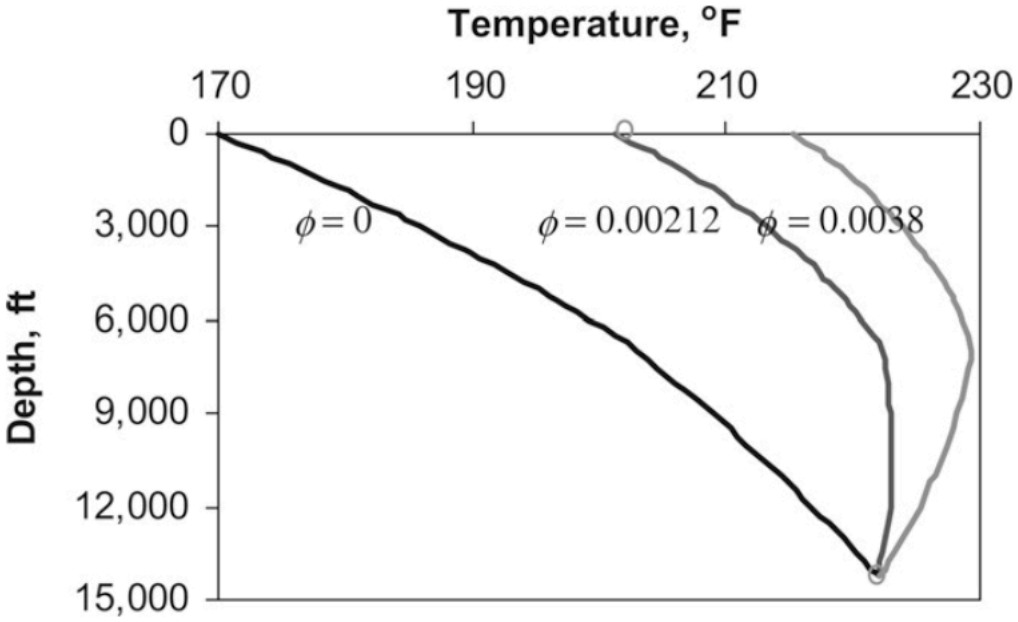

Figure 2-4 Effects of Varying ϕ (Hasan et al., 2009)

Figure 2-4 shows the effect of varying ϕ.

2.4.4 Heat Transfer in the Annulus

Stefan-Boltzmann's law gives the radiant heat flux between the outside surface of the tubing having temperature T_{to}, and the inside surface of the casing having temperature T_{ci} (Willhite, 1967):

$$Q_r = 2\pi r_{to}\sigma F_{tci}(T_{to}^{*4} - T_{ci}^{*4})\Delta L \qquad \textbf{(23)}$$

Where

Q_r = Annulus heat flow due to radiation (Btu/hr)

σ = Stephan-Boltzmann constant (=1.713×10^{-9} ft^2-hr-R^4)

T_{to} = Tubing outside temperature at surface (°F)

T_{ci} = Casing inside temperature at surface (°F)

ΔL = Length increment of tubing or casing (ft)

The asterisks at the temperatures mean that they are calculated with absolute temperature. F_{tci} is a view factor that connects the geometry of the wellbore and emissivity of the tubing and casing to the radiant heat flux (Willhite, 1967):

$$F_{tci} = \left[\frac{1}{\varepsilon_{to}} + \frac{r_{to}}{r_{ci}} \left(\frac{1}{\varepsilon_{ci}} - 1 \right) \right]^{-1} \quad \textbf{(24)}$$

Where

F_{tci} = View factor (dimensionless)

ε_{to} = Tubing outside emissivity at surface (dimensionless)

ε_{ci} = Casing inside emissivity at surface (dimensionless)

The heat transfer coefficient for radiation is defined as (Willhite, 1967):

$$h_r = \sigma F_{tci} (T_{to}^{*2} + T_{ci}^{*2})(T_{to}^{*} + T_{ci}^{*}) \quad \textbf{(25)}$$

Where

h_r = Radiative heat transfer coefficient (Btu/hr-ft^2-°F)

The expression for heat flux by radiation becomes (Willhite, 1967):

$$Q_r = 2\pi r_{to} h_r (T_{to}^{*} - T_{ci}^{*}) \Delta L \quad \textbf{(26)}$$

Heat transfer by convection and conduction occurs between the outside tubing surface and the inside casing surface (Willhite, 1967):

$$Q_c = 2\pi r_{to} h_c (T_{ci} - T_{to}) \Delta L \quad \textbf{(27)}$$

Where

Q_c = Annulus heat flow due to natural convection and conduction (Btu/hr)

h_c = Convective heat transfer coefficient (Btu/hr-ft^2-°F)

The heat transfer coefficient for convection and conduction is defined as (Willhite, 1967):

$$h_c = \frac{k_{hc}}{r_{to} \ln \frac{r_{ci}}{r_{to}}} \quad \textbf{(28)}$$

Where

k_{hc} = Equivalent thermal conductivity of annular fluids (Btu/hr-ft-°F)

$$\frac{k_{hc}}{k_{ha}} = 0.049(Gr \Pr)^{0.333} \Pr^{0.074} \quad \textbf{(29)}$$

Where

k_{ha} = Thermal conductivity of annular fluids (Btu/hr-ft-°F)

Gr = Grashof number (dimensionless)

$\Pr$ = Prandtl number (dimensionless)

The number 0.049 is found by Dropkin and Somerscales, and is applicable for $5\times10^4<\text{GrPr}<7.17\times10^8$ and vertical wells. An extrapolation is needed for deviated wells, with the following values given (Dropkin and Somerscales, 1965):

Table 2-2 C-values for Certain Well Inclinations

θ (degrees)	Corresponding C (dimensionless)
0	0.069
30	0.065
45	0.059
60	0.057
90	0.049

$$Gr = \frac{\left(r_{ci} - r_{to}\right)^3 g \rho_{an}^2 \beta \left(T_{to} - T_{ci}\right)}{\mu_{an}^2} \quad \textbf{(30)}$$

Where

g = Acceleration due to gravity (=4.17×10^8 ft/hr^2)

ρ_{an} = Annulus fluid density (lb/ft^3)

β = Thermal volumetric expansion coefficient of annulus fluid (°R^{-1})

μ_{an} = Annulus fluid viscosity (lbm/ft-hr)

$$\mathrm{Pr} = \frac{c_{an}\mu_{an}}{k_{ha}} \tag{31}$$

Where

c_{an} = Annulus fluid heat capacity (Btu/lb-°F)

For an ideal gas, the following expression gives the thermal volumetric expansion coefficient, β (Willhite, 1967):

$$\beta = \frac{1}{T^*_{an}} \tag{32}$$

Where

T^*_{an} = Average temperature of the fluid in the annulus (°R)

The general equation for β is given as (Willhite, 1967):

$$\beta = -\frac{1}{\rho_{an}}\left(\frac{\partial \rho_{an}}{\partial T}\right)_P \tag{33}$$

Where

P = Annulus pressure (psi)

2.4.5 Vertical Heat Transfer

The type of heat loss that most temperature models account for is radial heat loss to the surrounding formation. In some cases, for example a shut-in test, the wellbore

does not only lose heat to the surrounding formation radially, but also to the grid cells that are above and below, i.e. vertical heat transfer. This is a very important subject, especially for offshore wells (Izgec, 2008).

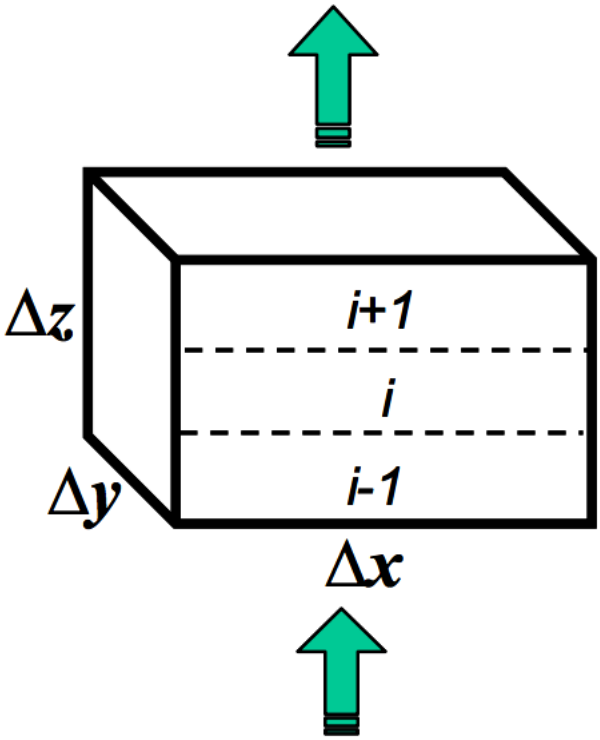

Figure 2-5 Control Volume for Vertical Heat Conduction (Izgec, 2008)

From Fourier's law, the amount of heat coming in and going out from "i" can be calculated (Izgec, 2008):

$$\frac{dQ_{in}}{dz} = -kA\frac{T_{i-1}^{n} - T_{i}^{n}}{\Delta z} \tag{34}$$

$$\frac{dQ_{out}}{dz} = -kA\frac{T_{i}^{n} - T_{i+1}^{n}}{\Delta z} \tag{35}$$

Where

$\frac{dQ_{in}}{dz}$ = Rate of heat coming in (Btu/hr)

$\frac{dQ_{out}}{dz}$ = Rate of heat coming out (Btu/hr)

A = Heat flow area (ft^2)

T = Temperature (°F)

From an energy balance for the volume element in addition to integration over time, and the introduction of the conduction term the following equation is obtained (Izgec, 2008):

$$kA\frac{\Delta T}{\Delta z^2} = kA\frac{T_{i+1}^n - 2T_i^n + T_{i-1}^n}{\Delta z^2} \quad \textbf{(36)}$$

From equation (36) the fluid temperature equation can be obtained (Izgec, 2008):

$$T_f = Ce^{-a't} + T_{ei} + kA\frac{\Delta T}{\Delta z^2}\frac{1}{mc_p(1+C_T)a'} \quad \textbf{(37)}$$

$$a' = \frac{L_R^{'}}{m(1+C_T)} \quad \textbf{(38)}$$

$$L_R^{'} = \frac{2\pi}{c_p}\left[\frac{r_{to}U_{to}k_e}{k_e + r_{to}U_{to}T_D}\right] \quad \textbf{(39)}$$

Where

C = Integration constant

C_T = Thermal storage parameter

The integration constant, C, can be written as the following when the initial condition after shut-in is applied (Izgec, 2008):

$$C = T_f^n - T_{ei} - kA\frac{\Delta T}{\Delta z^2}\left(L_R^{'}\right)^{-1} \quad \textbf{(40)}$$

3 Heat Transfer Model

The mathematics behind a temperature prediction model can be complex. Therefore, it is vital to establish a thorough and comprehensive background behind the equations and assumptions involved in the model. Figure 3-1 shows the way to draw the wellbore to fit the model.

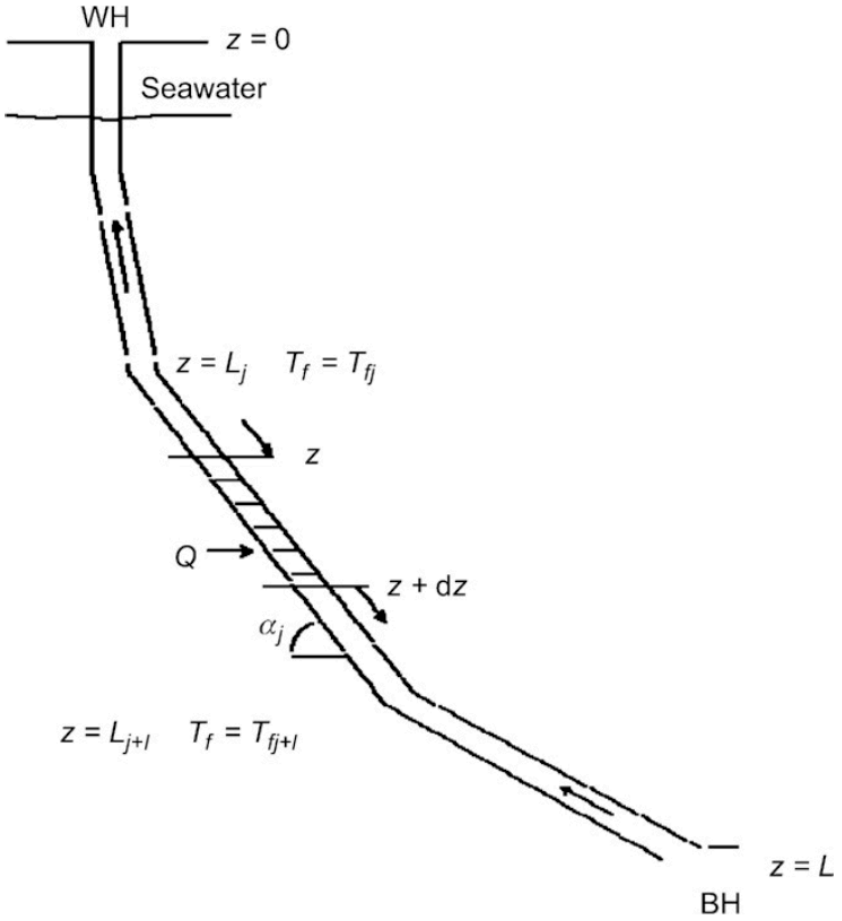

Figure 3-1 Wellbore Schematic (Hasan et al., 2009)

3.1 Initial and Boundary Conditions

Heat flux from the wellbore can be considered constant for a short time-step. The following differential equation can be used for formation temperature varying with radial distance from the wellbore (Hasan and Kabir, 1991):

$$\frac{\partial^2 T_e}{\partial r^2} + \frac{1}{r}\frac{\partial T_e}{\partial r} = \frac{c_e \rho_e}{k_e}\frac{\partial T_e}{\partial t} \qquad \textbf{(41)}$$

Where

r = Radial distance from wellbore (ft)

c_e = Formation heat capacity (Btu/lb-°F)

ρ_e = Density (lbm/ft^3)

If radial symmetry around a wellbore is assumed, unsteady-state three-dimensional heat diffusion can be treated as a two-dimensional problem. The initial conditions assumed are that the formation temperature remains time-invariable (Hasan and Kabir, 1991):

$$\lim_{t\to 0} T_e = T_{ei} \tag{42}$$

The boundary conditions assumed are that the formation temperature does not change with radial distance (Hasan and Kabir, 1991):

$$\lim_{r\to\infty} \frac{\partial T_e}{\partial r} = 0 \tag{43}$$

The other boundary condition comes from the heat flow rate where the formation and wellbore intersects. Fourier's law of heat conduction controls this (Hasan and Kabir, 1991):

$$\frac{dq}{dz} = -\frac{2\pi k_e}{W} \frac{r\,\partial T_e}{\partial r}\Big|_{r=r_{wb}} \tag{44}$$

3.2 Dimensionless Variables

Dimensionless variables are introduced to have a solution that is more applicable. r_D, t_D and α are introduced and inserted into equations (41), (43) and (44) (Hasan and Kabir, 1991):

$$r_D = \frac{r}{r_{wb}} \tag{45}$$

$$t_D = \frac{\alpha t}{r_{wb}^2} \tag{46}$$

$$\alpha = \frac{k_e}{\rho_e c_e} \tag{47}$$

Where

r_D = Dimensionless radius

t_D = Dimensionless time

α = Formation heat diffusivity (ft^2/hr)

t = Time (sec)

$$\frac{\partial^2 T_e}{\partial r_D^2} + \frac{1}{r_D}\frac{\partial T_e}{\partial t_D} = \frac{\partial T_e}{\partial t_D} \tag{48}$$

$$\lim_{r_D \to \infty} \frac{\partial T_e}{\partial r_D} = 0 \tag{49}$$

$$\frac{\partial T_e}{\partial r_D}\Big|_{r_D=1} = -\frac{W\left(\frac{dq}{dz}\right)}{2\pi k_e} \tag{50}$$

Equations (48), (49) and (50) lead to the following definition for dimensionless temperature (Hasan and Kabir, 1991):

$$T_D = -\frac{2\pi k_e}{W(dq/dz)}\left(T_{wb} - T_{ei}\right) \tag{51}$$

Where

T_D = Dimensionless temperature

Using these conditions, Hasan and Kabir reached a solution for the dimensionless temperature equation (Hasan and Kabir, 1991):

$$T_D = 1.1281\sqrt{t_D}\left(1-0.3\sqrt{t_D}\right),\ 10^{-10} \le t_D \le 1.5 \quad \textbf{(52)}$$

$$T_D = \left(0.4063+0.5\ln(t_D)\right)\left(1+\frac{0.6}{t_D}\right),\ t_D > 1.5 \quad \textbf{(53)}$$

3.3 Casing and Wellbore Temperatures

After defining the initial and boundary conditions, the casing and wellbore temperatures need to be found. Based on the equation for rate of heat transfer between a flowing fluid and the inside of a tubing wall, the equations for casing temperatures can be obtained. Starting with (Willhite, 1967):

$$Q = 2\pi r_{to} U_{to}(T_f - T_h)\Delta L \quad \textbf{(54)}$$

Where

T_h = Cement-formation interface temperature (°F)

Combining equation (54) with heat transfer for conduction through casing and cement gives (Willhite, 1967):

$$Q_{cas} = \frac{2\pi k_{cas}(T_{ci} - T_{co})\Delta L}{\ln\frac{r_{co}}{r_{ci}}} \quad \textbf{(55)}$$

$$Q_{cem} = \frac{2\pi k_{cem}(T_{co} - T_h)\Delta L}{\ln\frac{r_h}{r_{co}}} \quad \textbf{(56)}$$

Where

Q_{cas} = Heat flow casing (Btu/hr)

Q_{cem} = Heat flow cement (Btu/hr)

r_h = Drill hole radius (ft)

T_{co} = Outside casing temperature (°F)

The following equation is then obtained for the casing temperature (Willhite, 1967):

$$T_{ci} = T_h + \left(\frac{\ln \frac{r_h}{r_{co}}}{k_{cem}} + \frac{\ln \frac{r_{co}}{r_{ci}}}{k_{cas}} \right) r_{to} U_{to} (T_f - T_h) \quad \textbf{(57)}$$

The outside casing temperature is given by (Tøien, 2015):

$$T_{co} = T_{wb} + \frac{r_{to} U_{to}}{r_{co} \left(h_r + h_c \right)} \left(T_f - T_{wb} \right) \quad \textbf{(58)}$$

T_h is given by (Willhite, 1967):

$$T_h = \frac{T_f T_D + \frac{k_e T_e}{r_{to} U_{to}}}{T_D + \frac{k_e}{r_{to} U_{to}}} \quad \textbf{(59)}$$

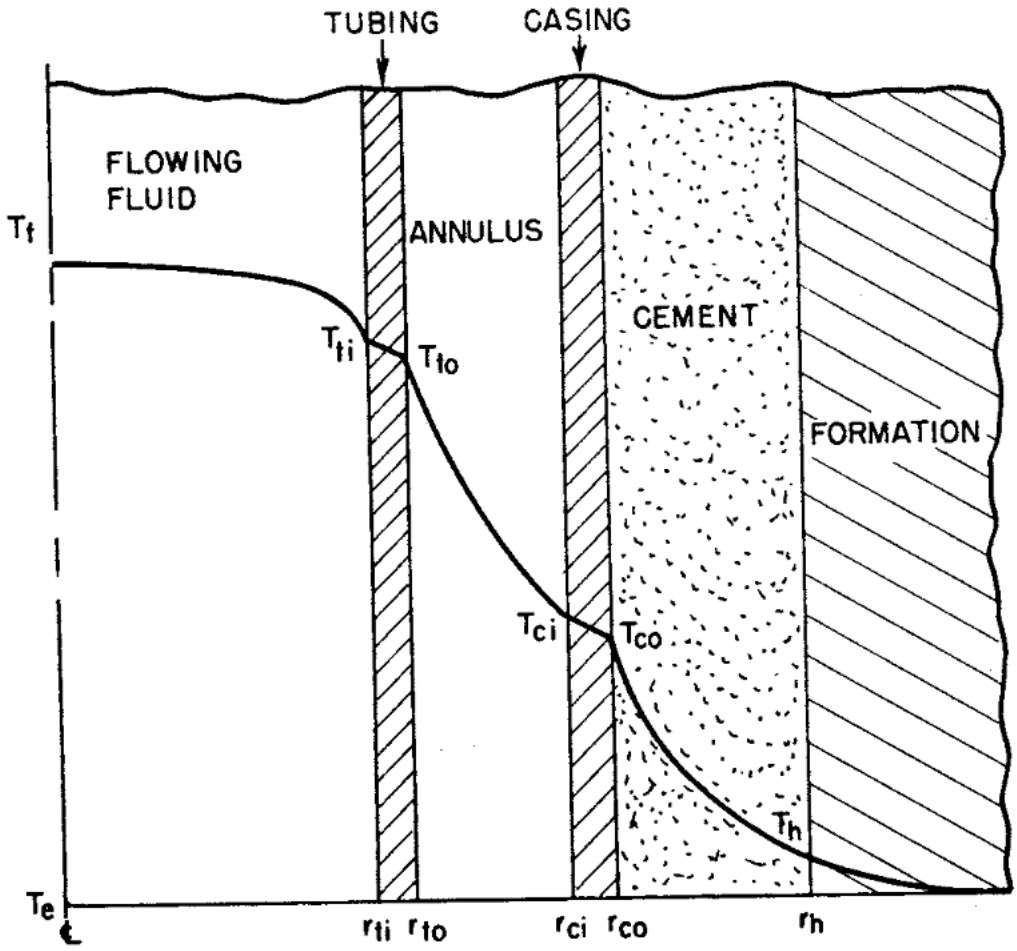

Figure 3-2 Temperature Distribution (Willhite, 1967)

3.4 Stepwise Temperature Modeling

The well needs to be divided into several sections to calculate the correct temperatures, because the equations will be different for parts of the well that have different interfaces. It is assumed that both the surface casing and the conductor casing are cemented to the top, while the intermediate and production casing and the production liner are cemented for a specified length. Iterations are needed to calculate the correct values for the overall heat transfer coefficient for each section, and therefore also the heat transfer coefficients in the annuli.

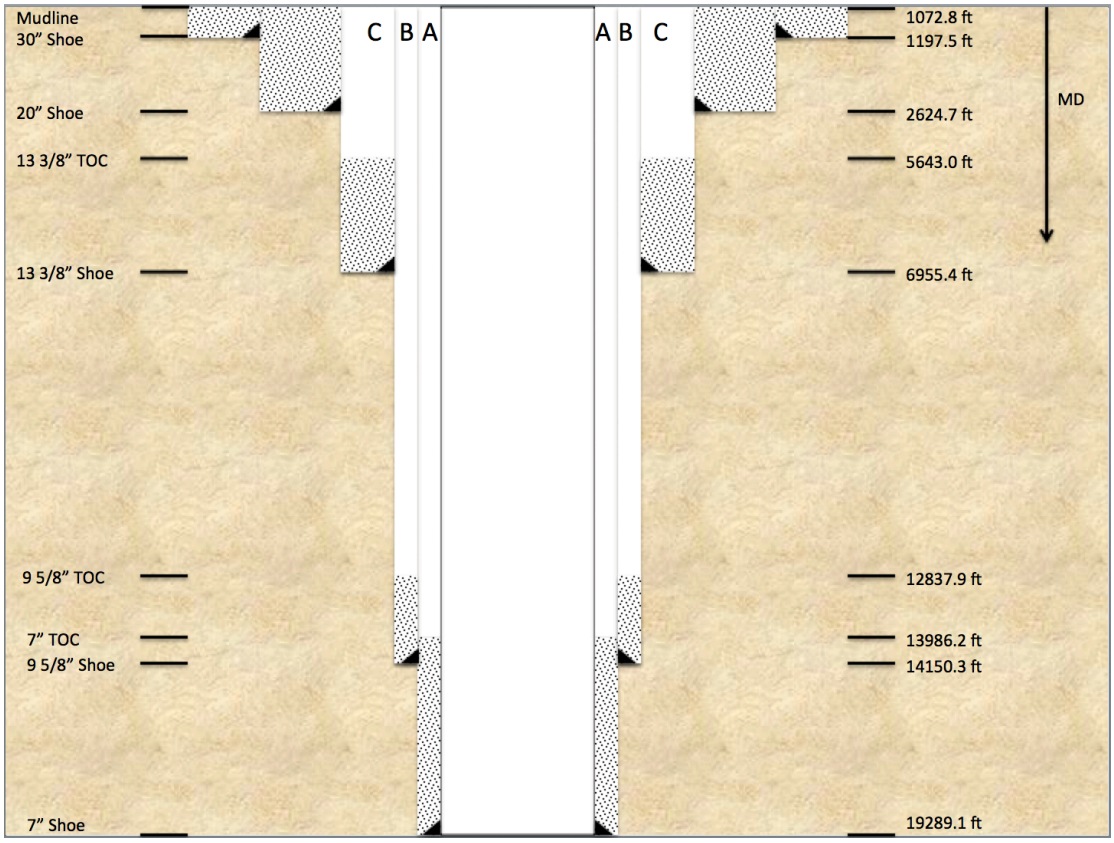

Figure 3-3 Well Schematic

Table 3-1 Casing and Tubing Diameter Dimensions

Type	Pipe Diameter (in)	Hole Diameter (in)
Conductor Casing	30	36
Surface Casing	20	26
Intermediate Casing	13 3/8	17 1/2
Production Casing	9 5/8	12 1/4
Production Liner	7	8 1/2

The well is being iterated for each foot. Figure 3-3 shows the schematic for the well used in the simulations, and is based on the well schematic from WellCat. The A, B and C on the schematic represent the A-, B- and C-annulus of the well. The equations that vary for each section are the following: U_{to}, T_{ci} and T_{co}, from equations (15), (57) and (58) respectively. T_{wb} is given by equation (59). These equations lead to a calculation of T_f from equation (21). The following will explain the steps to model the temperature prediction for flowing fluid temperatures, where the figures are based on Figure 3-2 from Willhite's paper from 1967. The temperature decreases from left to right on the figure for each of the steps, with flowing fluid temperature in green, casing and tubing inside and outside temperatures in blue and wellbore temperature in red. Resulting equations used in the model for U_{to} can be found in Appendix B.

3.4.1 Step 1

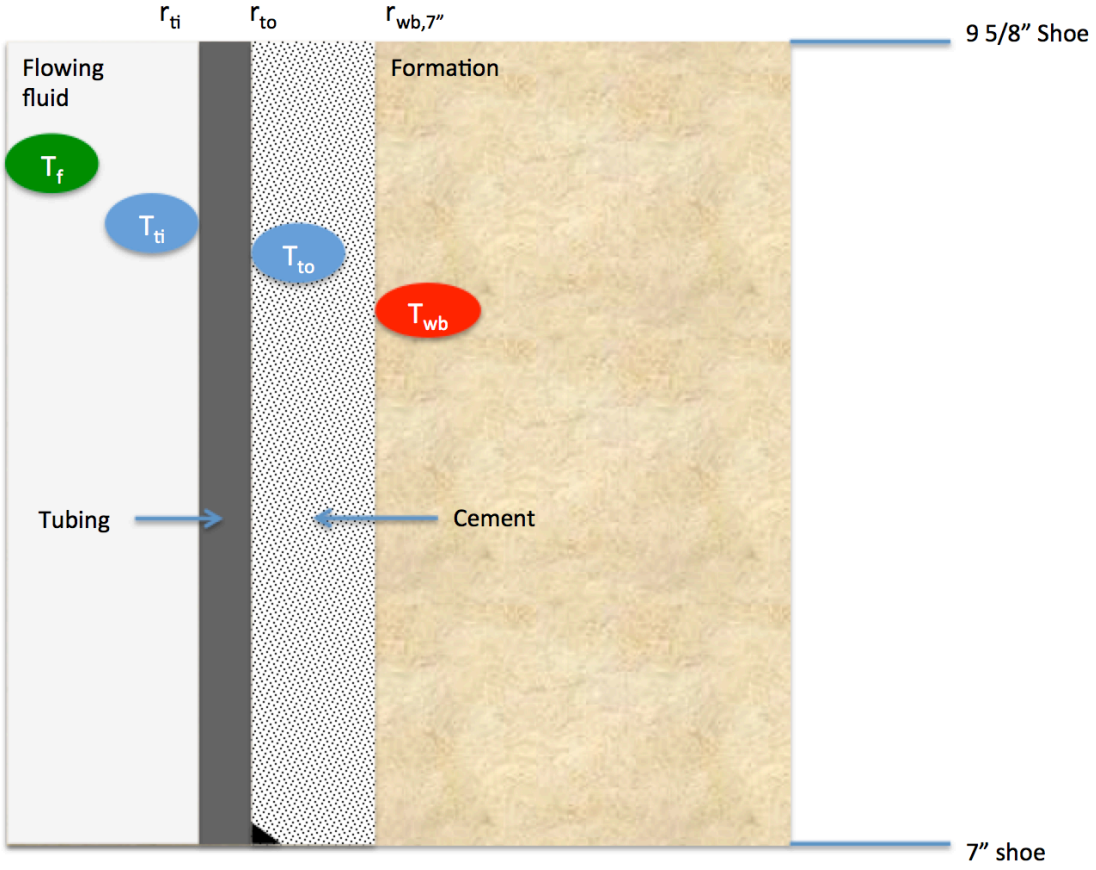

Figure 3-4 Step 1 for the Model

The first step in the model is to calculate the equations from the shoe of the production tubing and up to the shoe of the production casing. This section has a flowing fluid in the tubing, cement outside the tubing and no annulus.

U_{to} is calculated with a constant equation for this section, due to no annulus. The value for T_f will be iterated for each foot of the section.

3.4.2 Step 2

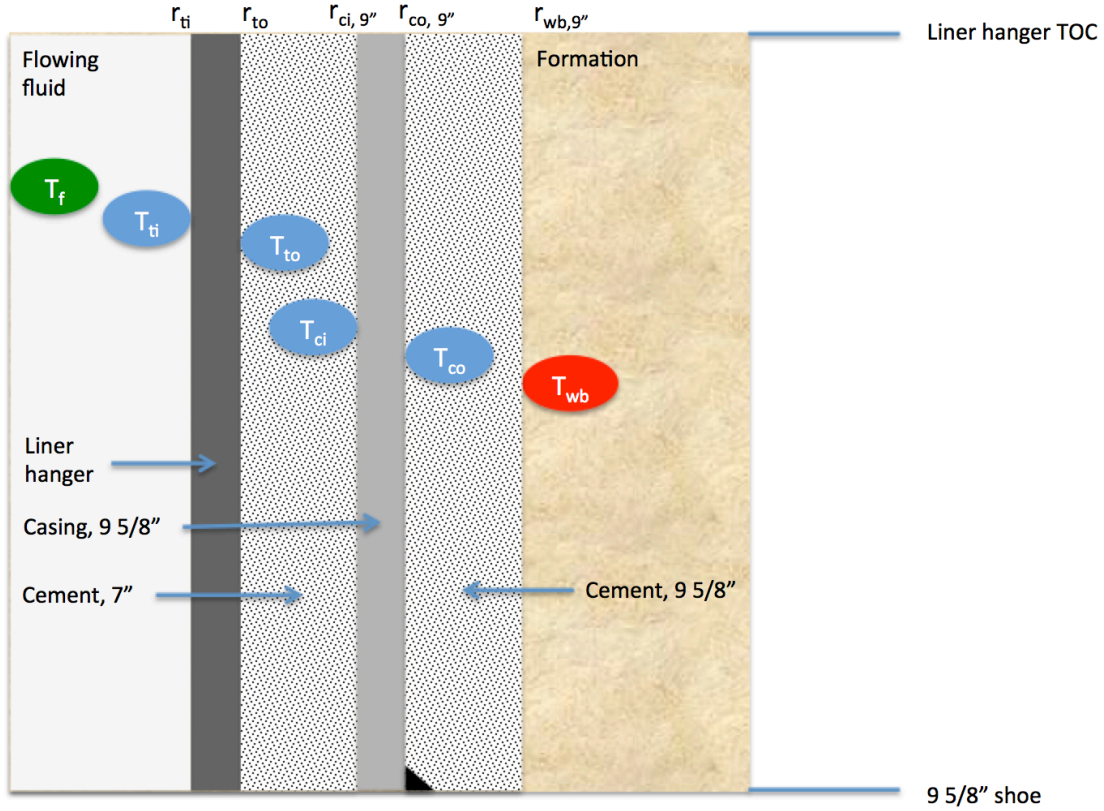

Figure 3-5 Step 2 for the Model

The second step is to calculate the equations from the production casing shoe to the top of cement of the liner hanger. This section has cement outside both the liner hanger and the production casing. The outside and inside temperatures for the production casing are assumed to be equal, because of the cement on both sides. U_{to} is calculated with a constant equation for this section as well, due to no annulus.

3.4.3 Step 3

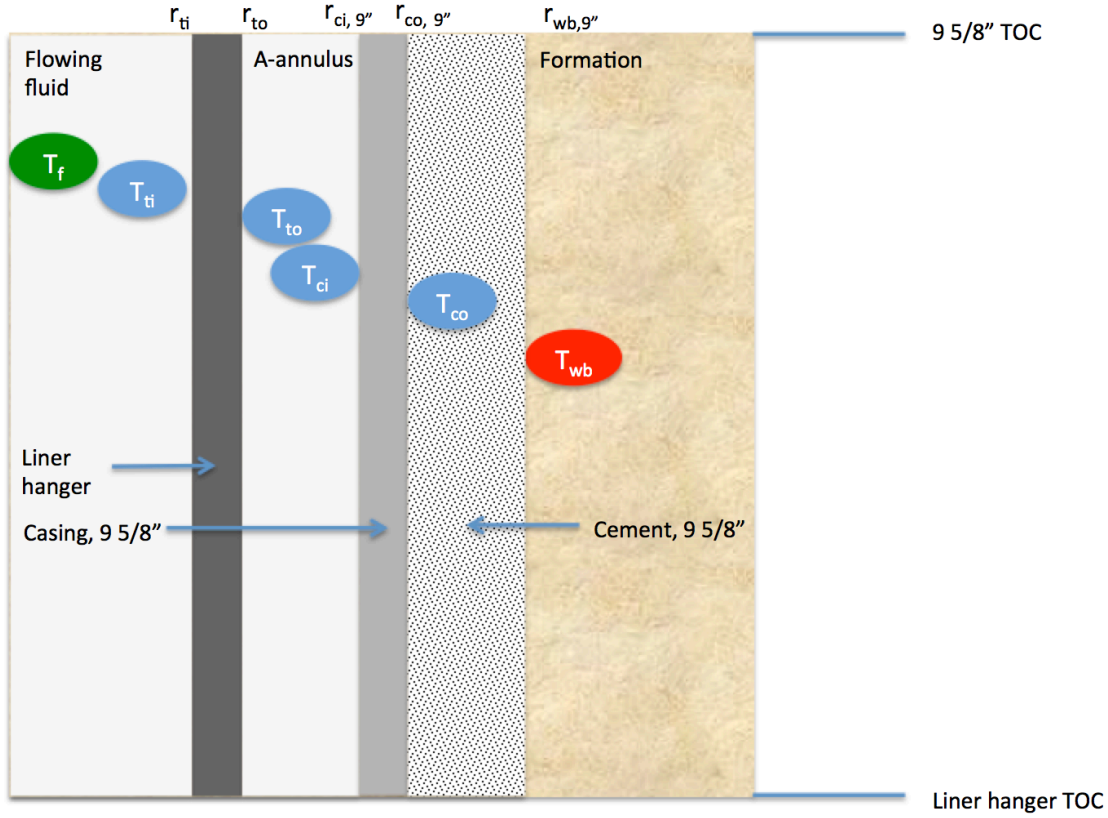

Figure 3-6 Step 3 for the Model

The third step is to calculate the equations from the top of cement of the liner hanger to the top of cement of the production casing. This section has an annulus between the liner hanger and the casing, so the heat transfer due to convection and radiation in the annulus needs to be taken into account. Therefore, U_{to} and the outside casing temperature need to be checked for convergence. When the convergence is reached for the outside casing temperature, U_{to} can be calculated. When U_{to} has reached convergence, T_f can be calculated.

3.4.4 Step 4

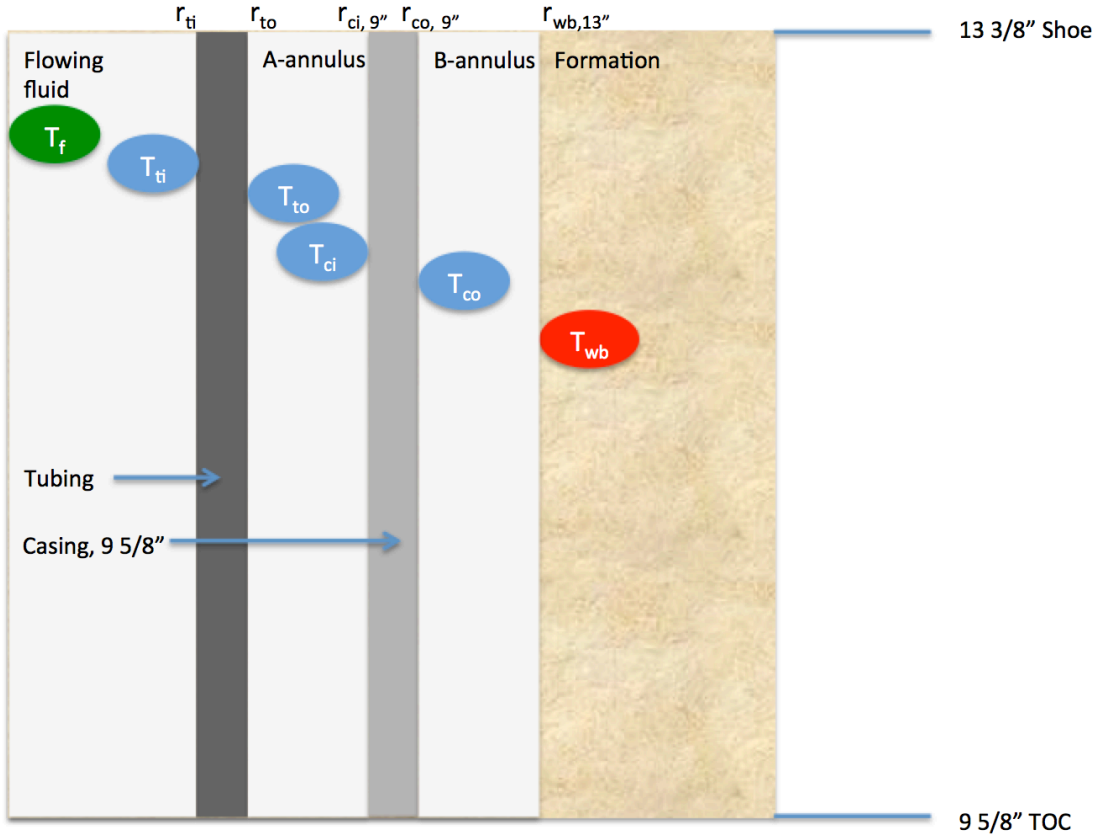

Figure 3-7 Step 4 for the Model

The fourth step is to calculate the equations from the top of cement of the production casing to the shoe of the intermediate casing. This section has two annuli. Therefore, the heat transfer due to convection and radiation needs to be taken into account in both annuli. U_{to} and the outside casing temperature need to be checked for convergence in the same way as in step 3, before T_f can be calculated.

3.4.5 Step 5

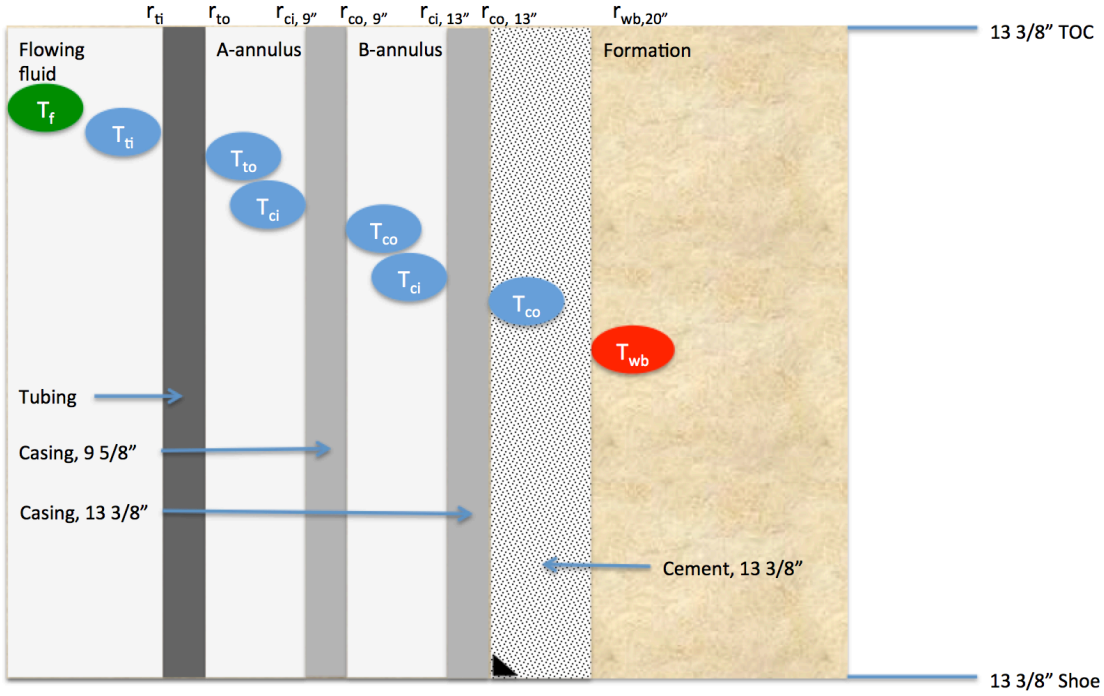

Figure 3-8 Step 5 for the Model

The fifth step is to calculate the equations from the shoe of the intermediate casing to the top of cement of the intermediate casing. The section has two annuli and cement outside the intermediate casing. The outside intermediate casing accounts for the heat transfer through the cement. Heat transfer due to convection and radiation in the annulus is taken into account. U_{to} and the outside production casing temperature need to be checked for convergence in the same way as in step 3, before T_f can be calculated.

3.4.6 Step 6

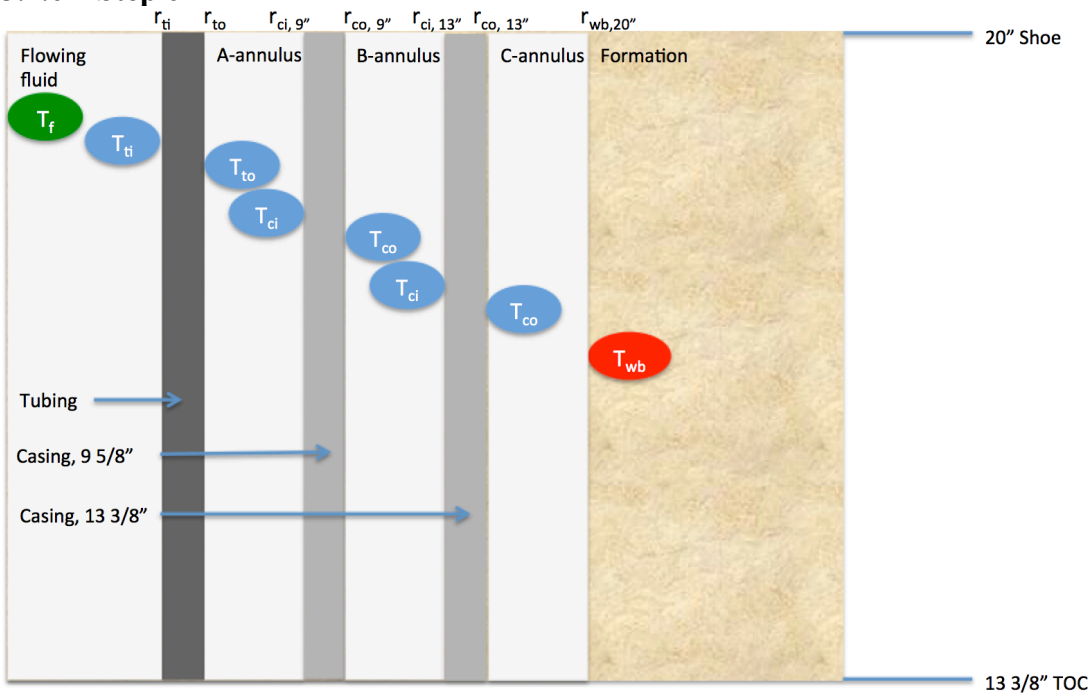

Figure 3-9 Step 6 for the Model

The sixth step is to calculate the equations from the top of cement of the intermediate casing to the shoe of the surface casing. This section has three annuli. Heat transfer due to convection and radiation needs to be taken into account in all three annuli. The outside intermediate casing temperature is first checked for convergence. Then the outside production casing temperature is checked for convergence, and U_{to} is finally checked for convergence before T_f can be calculated.

3.4.7 Step 7

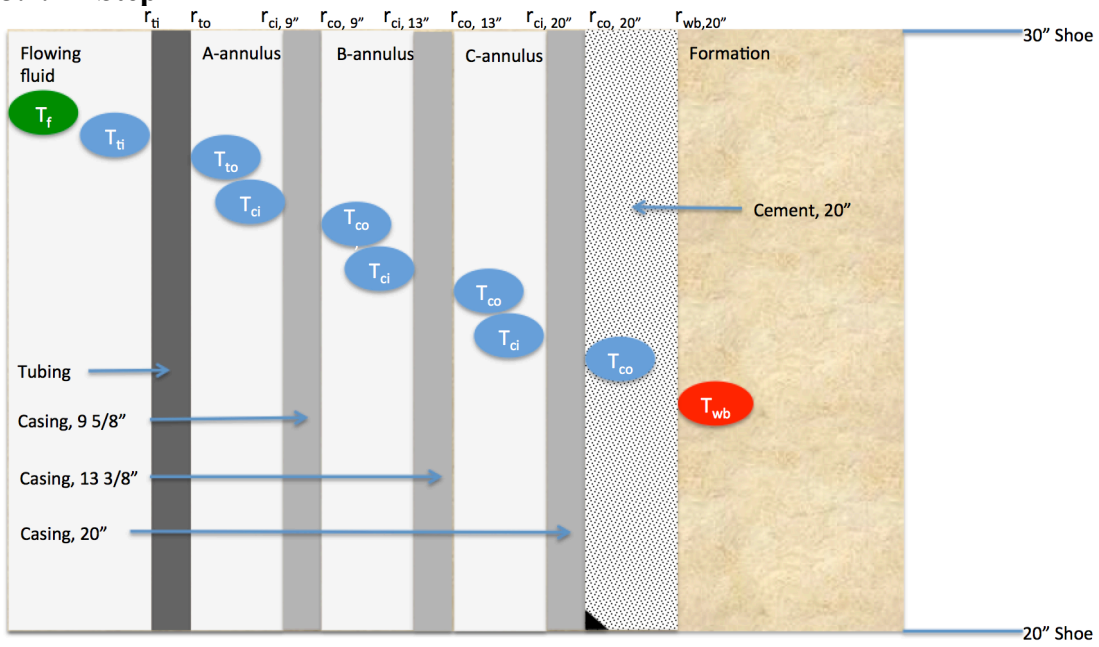

Figure 3-10 Step 7 for the Model

The seventh step is to calculate the equations from the shoe of the surface casing to the shoe of the conductor casing. This section has three annuli and cement outside the surface casing. The outside surface casing temperature accounts for the heat transfer through the cement. Heat transfer due to convection and radiation needs to be taken into account in all three annuli. The outside intermediate casing temperature is first checked for convergence. Then the outside production casing temperature is checked for convergence, and U_{to} is finally checked for convergence before T_f can be calculated.

3.4.8 Step 8

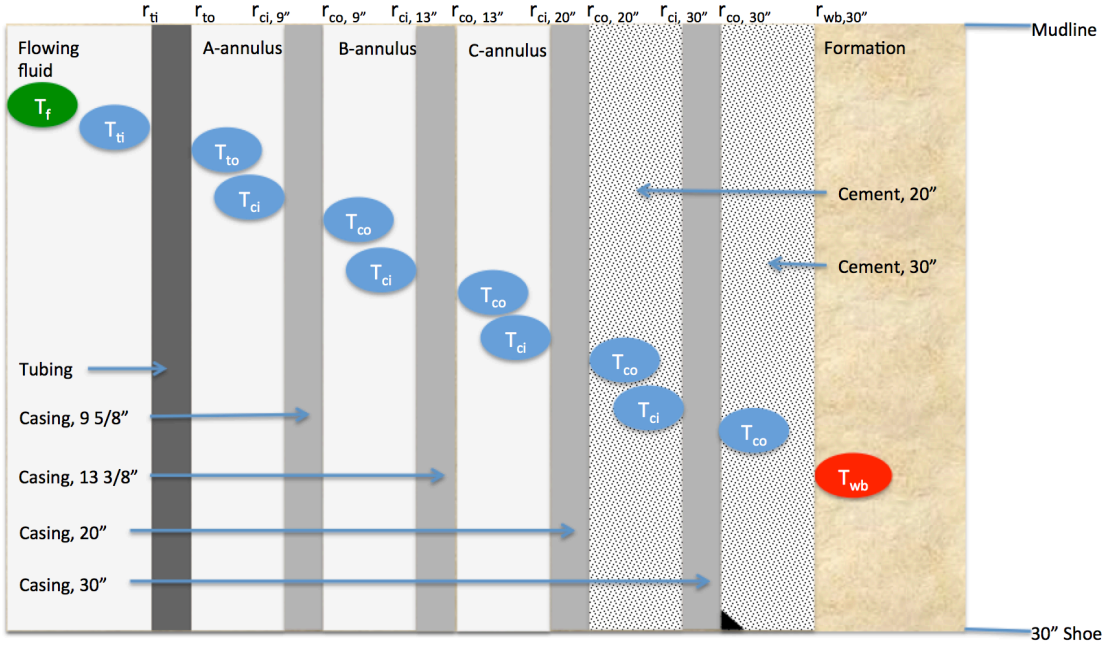

Figure 3-11 Step 8 for the Model

The eight and final step is to calculate the equations from the shoe of the conductor casing to the mudline. This section has three annuli and cement outside both the surface casing and conductor casing. The outside surface casing temperature accounts for the heat transfer through both layers of cement. Heat transfer due to convection and radiation needs to be taken into account in all three annuli. The outside intermediate casing temperature is first checked for convergence. Then the outside production casing temperature is checked for convergence, and U_{to} is finally checked for convergence before T_f can be calculated.

The eight steps are summed up in a flowchart of the model in Figure 3-12.

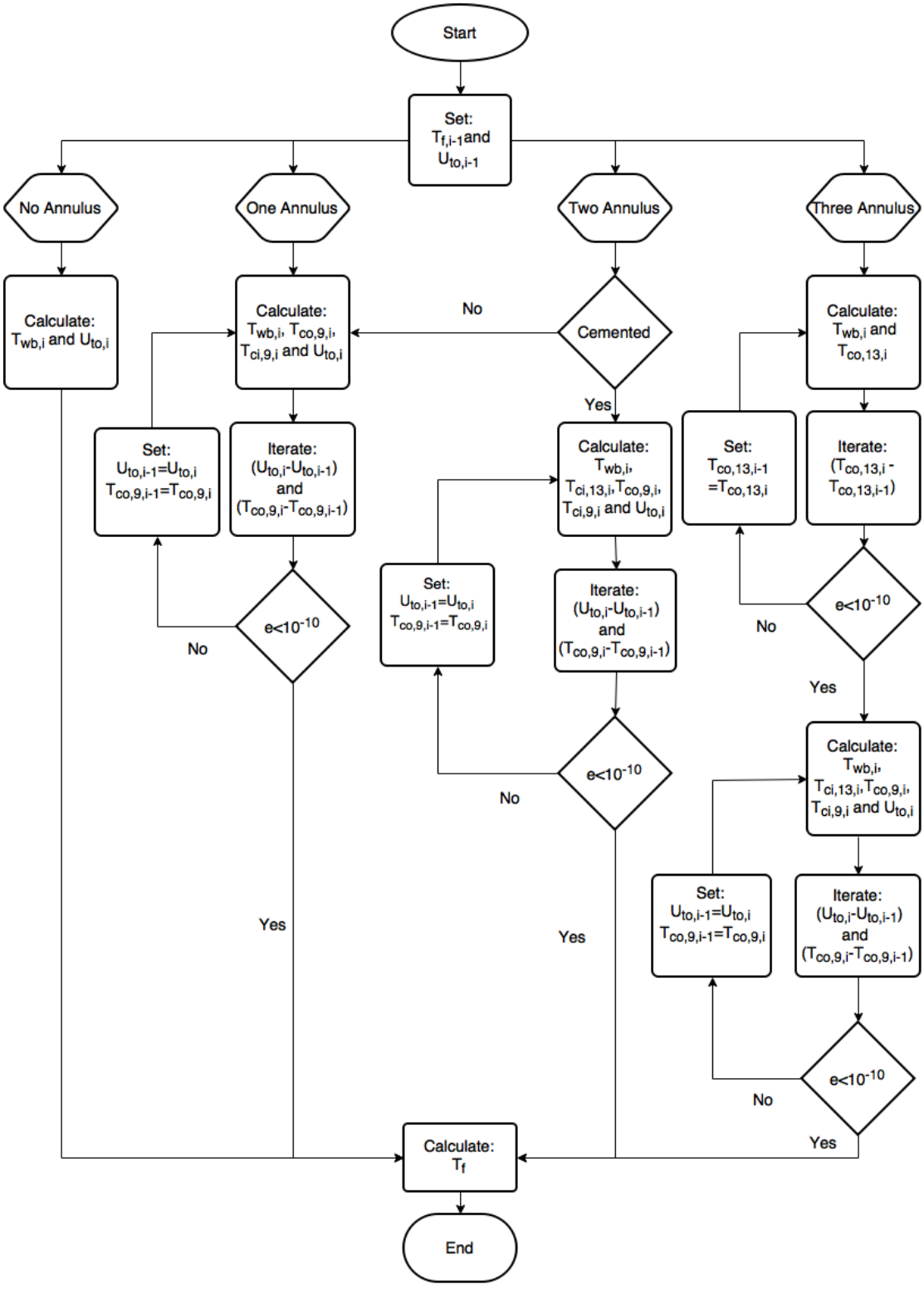

Figure 3-12 Flowchart for Fluid Temperature Prediction

4 Vertical Heat Transfer Model

Implementing a vertical heat transfer model involves numerical differentiation and matrix calculations. A brief explanation of how to implement it is given below.

4.1 Initial and Boundary Conditions

The following initial and boundary conditions are applicable for this model (Izgec, 2008):

$$\begin{aligned} T(r,0) &= T_{ei} \\ T(r=r_t) &= T_f(t) \\ T(r=\infty,t) &= T_{ei} \end{aligned} \qquad \textbf{(60)}$$

Where

r_t = Tubing outside radius (ft)

4.2 Mathematics

When developing a temperature model that includes vertical heat transfer, cylindrical grids represent the wellbore with radial grids around them. The radial grids surrounding the cylindrical grids are generated to calculate the heat flow from tubing fluid into the formation. These are generated in addition to solving for conduction equation in finite difference form (Izgec, 2008).

The accuracy of the finite difference solution is improved by making equally spaced nodes on a logarithmic basis. The analogy between heat and fluid flow equations makes it possible to generate radial grids around the wellbore that are geometrically spaced, which again makes it possible to calculate the formation temperatures. The outer boundary is the outer grid, which represents the geothermal gradient (Izgec, 2008).

Generating the radial grids consists of three calculation steps (Izgec, 2008):
Calculate a scaling parameter:

$$\beta = \left(\frac{r_e}{r_{wb}} \right)^{\frac{1}{i\max - 1}} \tag{61}$$

Calculate the initial grid distance:

$$r_{i+1} = \beta r_i \tag{62}$$

Calculate the remaining grids:

$$r_{i+\frac{1}{2}} = \beta r_{i-\frac{1}{2}} \tag{63}$$

$$r_i = \sqrt{r_{i+\frac{1}{2}} r_{i-\frac{1}{2}}} \tag{64}$$

Where

r_e = Maximum distance from wellbore to formation

$i\max$ = Number of grids around the wellbore

Using the heat conduction equations the following implicit equation for the temperature can be obtained, where "i" represents space and "n" represents time (Izgec, 2008):

$$TR_W T_{i-1}^{n+1} - TR_C T_i^{n+1} - TR_E T_{i+1}^{n+1} = -\frac{\alpha}{\Delta t} T_i^n \tag{65}$$

$$TR_W = \frac{2k_{i-1}\pi r_{i-1} h}{\Delta r_i} \tag{66}$$

$$TR_E = \frac{2k_i \pi r_i h}{\Delta r_{i+1}} \tag{67}$$

$$TR_C = TR_W - TR_E + \frac{\alpha}{\Delta t} \tag{68}$$

$$\alpha = c\rho\pi\Delta r^2 h \tag{69}$$

This implicit equation can be solved using matrix operations, and its matrix form is given as (Izgec, 2008):

$$\begin{vmatrix} 1 & & & \\ TR_W & TR_C & TR_E & \\ & TR_W & TR_C & TR_E \\ & & TR_W & TR_C \end{vmatrix} \bullet \begin{vmatrix} T_1^{n+1} \\ T_2^{n+1} \\ T_3^{n+1} \\ T_4^{n+1} \end{vmatrix} = -\frac{\alpha}{\Delta t} \begin{vmatrix} T_1^n \\ T_2^n \\ T_3^n \\ T_4^n \end{vmatrix} \tag{70}$$

This matrix is made for a case with four radial grids and one vertical wellbore grid.

5 Results

The model explained in Chapter 3 was implemented in Matlab to obtain the best possible understanding regarding temperature prediction problems and challenges. The input and well trajectory used in this thesis was also used in the courses TPG4525 Specialization Course and TPG4520 Specialization Project (Lervik, 2015).

5.1 Assumptions

The following assumptions were taken into account when making the model:

- Radial symmetry around wellbore
- Constant formation heat diffusivity
- Steady-state flow
- Single-phase flow
- Constant emissivities and conductivities
- Ideal gas

5.2 Input

Table 5-1 shows the casing and tubing configuration used in the model. These values were the result from the course TPG4525 Specialization Course.

Table 5-1 Casing and Tubing Configuration

Type	Pipe Diameter (in)	Hole Diameter (in)	Shoe Depth, TVD (ft)	Shoe Depth, MD (ft)	Inclination (degrees)	Top of Cement, MD (ft)
Conductor	30	36	1197.5	1197.5	0	1072.8
Surface	20	26	2624.6	2624.7	1.62	1072.8
Intermediate	13 3/8	17 1/2	6868.8	6955.4	19.03	5643.0
Production Casing	9 5/8	12 1/4	12934.4	14150.3	66.18	12837.9
Production Liner	7	8 1/2	13293.4	19289.1	89.9	13986.2

Table 5-2 shows the input variables that were used in the model. These were found from the specialization course and from the master's thesis of Knut Vegard Løbergsli (Løbergsli, 2015).

Table 5-2 Input of Variables for the Model

Variable	Value	Units
Conductivity casing, k_{cas}	26.2	Btu/hr-ft^2-°F
Conductivity tubing, k_{tub}	26.2	Btu/hr-ft^2-°F
Conductivity cement, k_{cem}	0.568	Btu/hr-ft^2-°F
Conductivity formation, k_e	0.92	Btu/hr-ft^2-°F
Conductivity annulus, k_{an}	0.35	Btu/hr-ft^2-°F
Emissivity, ε	0.85	Dimensionless
Heat diffusivity formation, α	0.022	ft^2/hr
Geothermal gradient, g_T	1.44	°F/100ft
Fluid density A-annulus, $\rho_{an,A}$	78.03	lbm/ft^3
Fluid density B-annulus, $\rho_{an,B}$	109.25	lbm/ft^3
Fluid density C-annulus, $\rho_{an,C}$	90.52	lbm/ft^3
Viscosity annulus, μ_{an}	60	lbm/ft-hr
Heat capacity annulus fluid, $c_{p,an}$	0.95	Btu/lbm-°F
Heat capacity flowing fluid, $c_{p,m}$	0.7	Btu/lbm-°F
Time, t	2000	hr
Mass flow rate, w_t	70	lbm/sec
Gravity acceleration, g_a	32.2	ft/sec^2

5.3 Results

The model was run to compare against results from the ILS and to check the sensitivity of certain variables.

5.3.1 Simulation Results

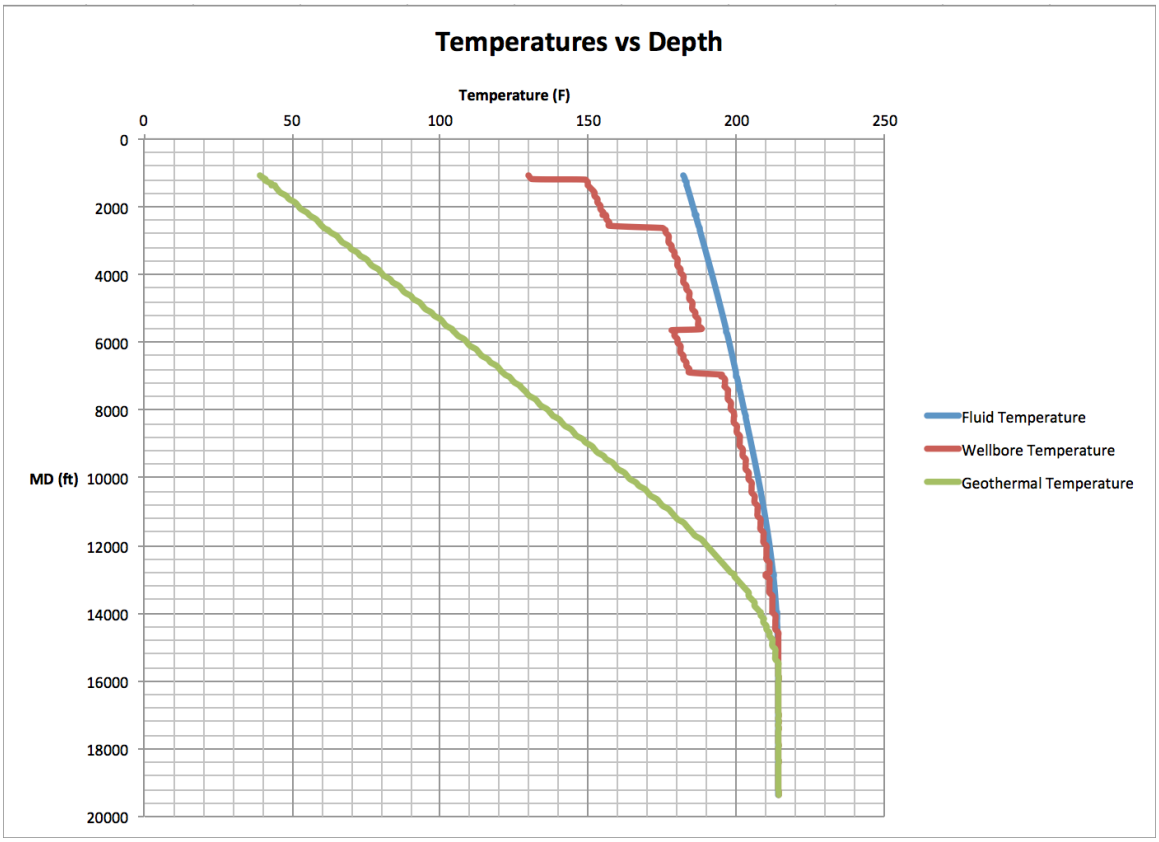

Figure 5-1 Simulated Temperatures vs. Measured Depth

Figure 5-1 shows the flowing fluid temperature in blue, wellbore temperature in red and the undisturbed geothermal temperature in green. The values are plotted against measured depth, and the values are the result from simulation in Matlab. The wellbore temperature showed increased temperatures below each casing shoe, and decreased temperatures where the casings were cemented. The values for all three temperatures showed constant values where the deviation of the well was 90 degrees, at around 15 000 feet.

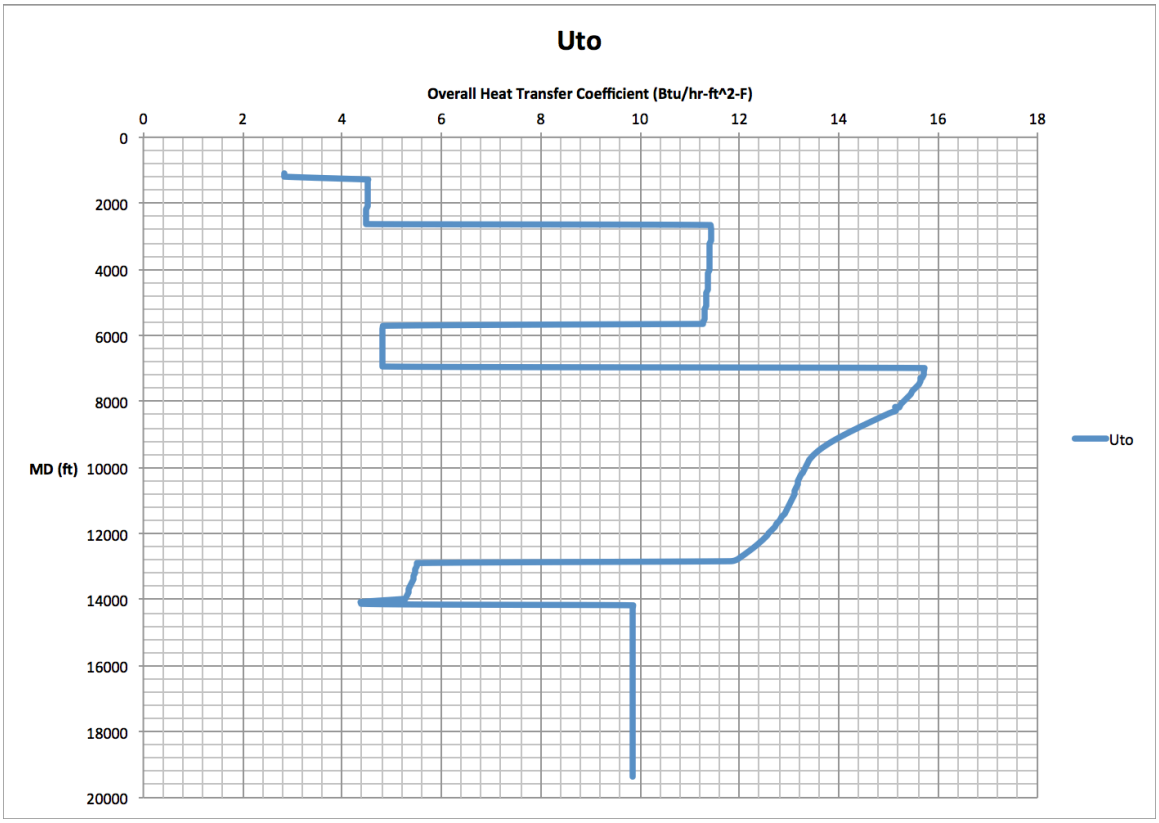

Figure 5-2 Overall Heat Transfer Coefficient vs. Measured Depth

Figure 5-2 shows the overall heat transfer coefficient for the simulated well. It increased below each casing shoe, and decreased where the casing was cemented. The highest value of the overall heat transfer coefficient was found just below the intermediate casing shoe. The lowest value was found at the mudline.

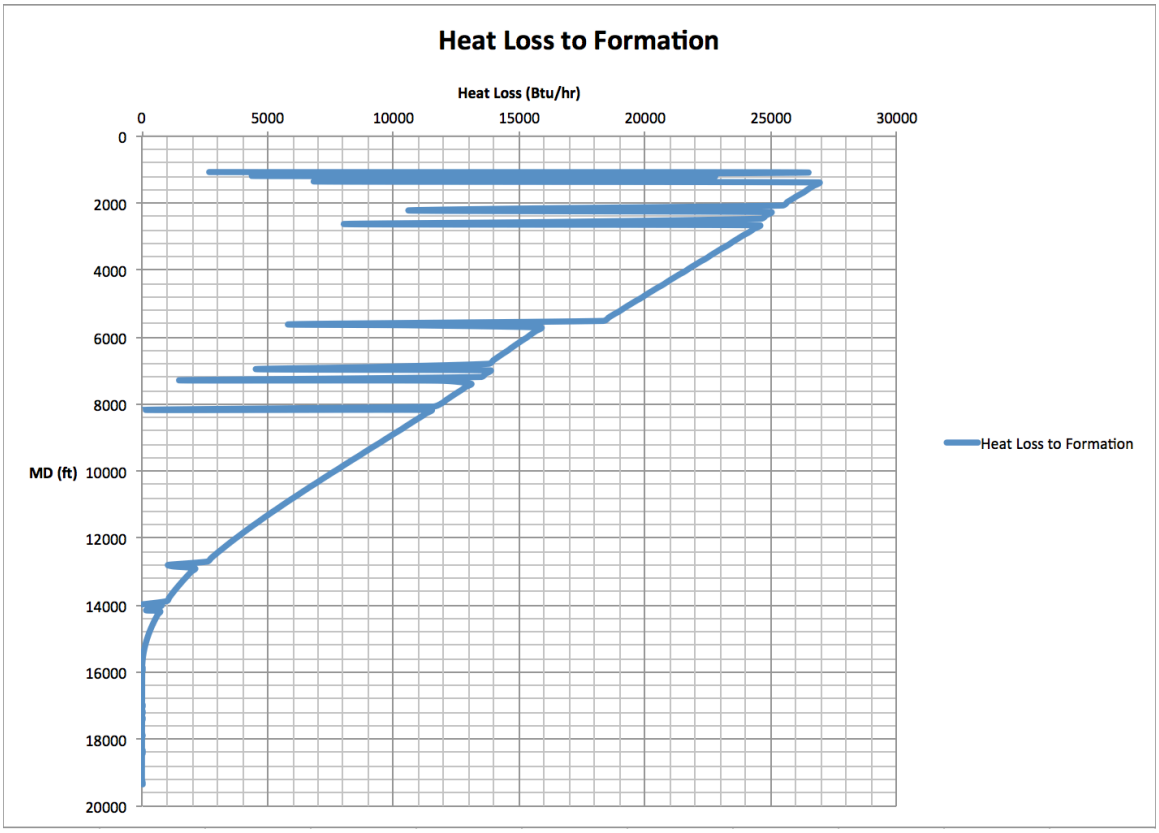

Figure 5-3 Heat Loss to Formation

Figure 5-3 shows the simulated heat loss to the formation in Btu/hr. The total simulated heat loss was 1 769 300 Btu/hr.

5.3.2 Simulation Results vs. ILS

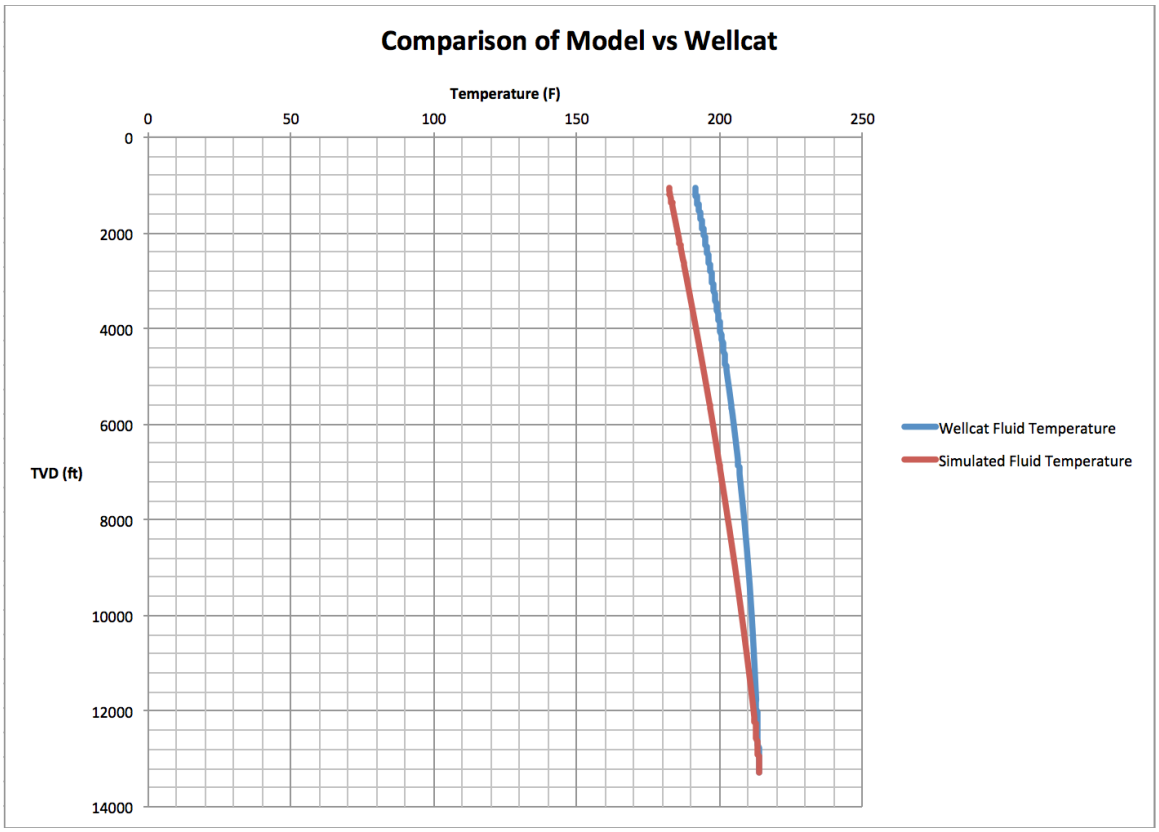

Figure 5-4 Comparison of Simulated Fluid Temperature vs. WellCat Fluid Temperature

Figure 5-4 shows a comparison of the simulated fluid temperature in red and the WellCat fluid temperature in blue. The simulated temperature was lower than the WellCat temperature for the entire well, except from at the bottom, where the simulated temperature was 0.5 °F higher.

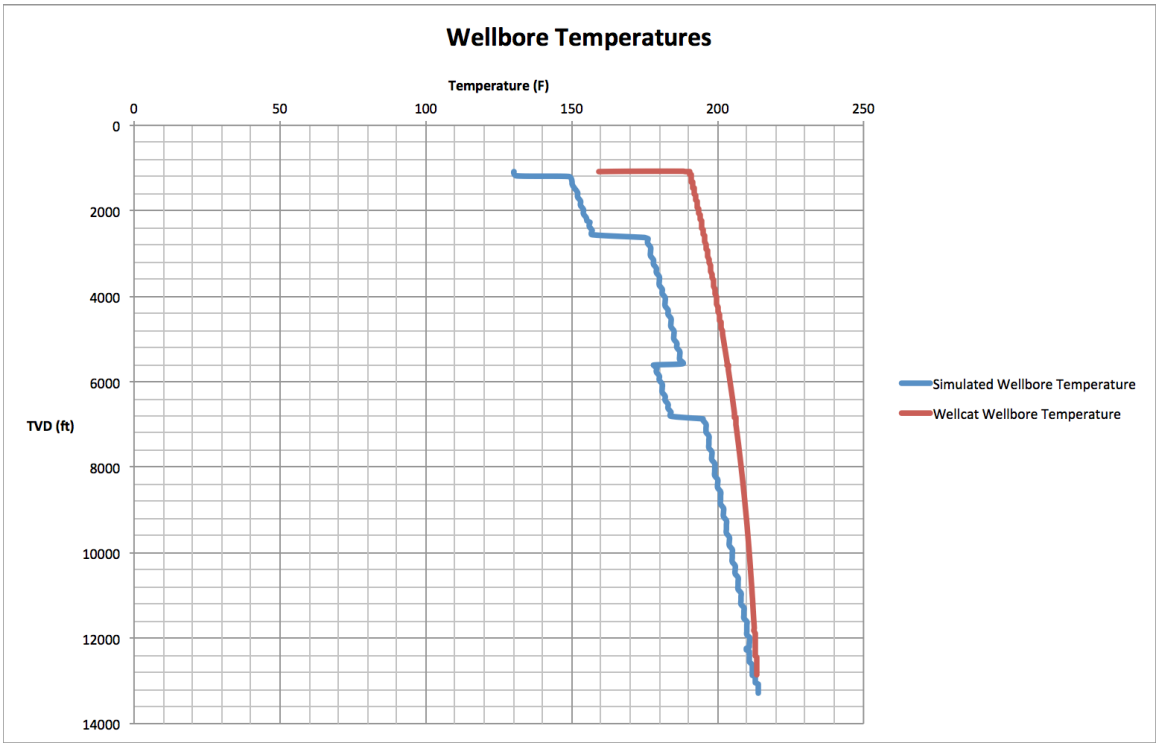

Figure 5-5 Comparison of Simulated Wellbore Temperature vs. WellCat Wellbore Temperature

Figure 5-5 compares the simulated wellbore temperature in blue to the WellCat wellbore temperature in red. The simulated temperature was lower than the WellCat temperature for the entire well.

5.3.3 Varying ϕ

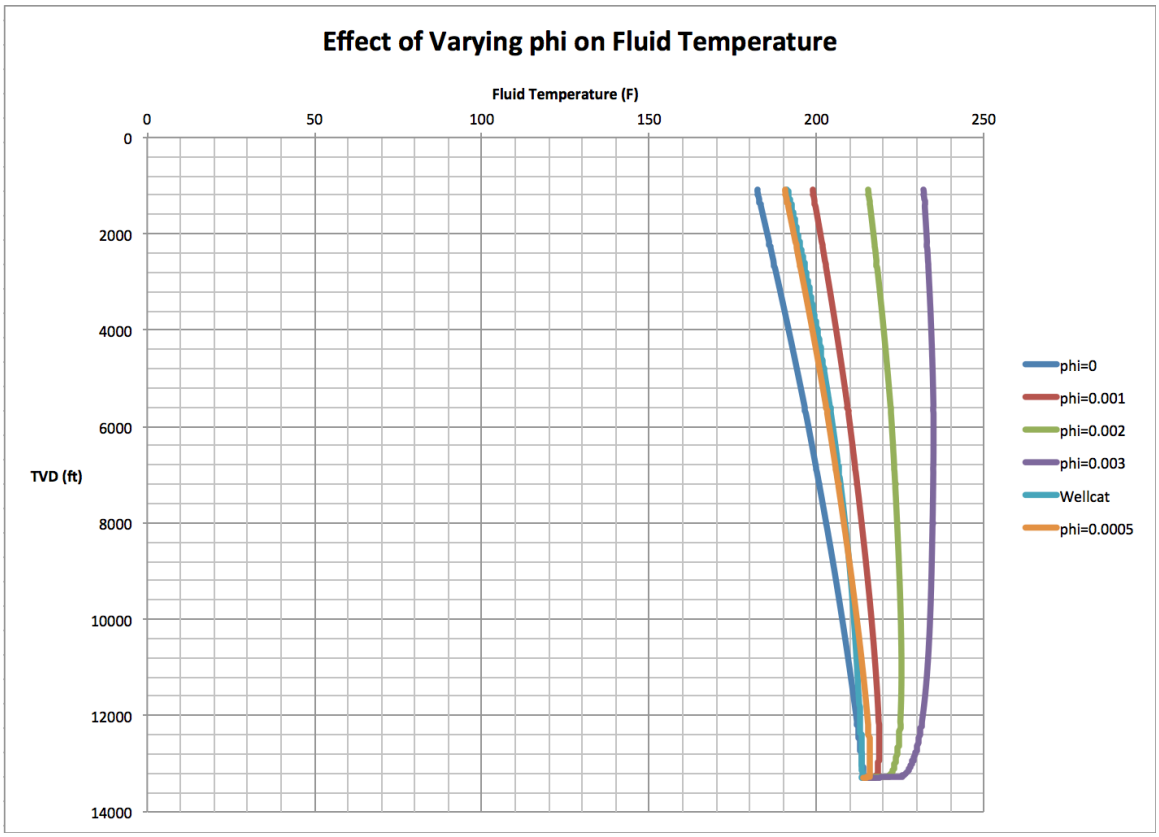

Figure 5-6 Effect of Varying ϕ on Fluid Temperature

Figure 5-6 shows the simulated fluid temperatures with varying ϕ, with ϕ=0, ϕ=0.0005, ϕ=0.001, ϕ=0.002 and ϕ=0.003, and the WellCat fluid temperature. ϕ=0 gave the lowest temperature with the temperature increasing for increasing values of ϕ.

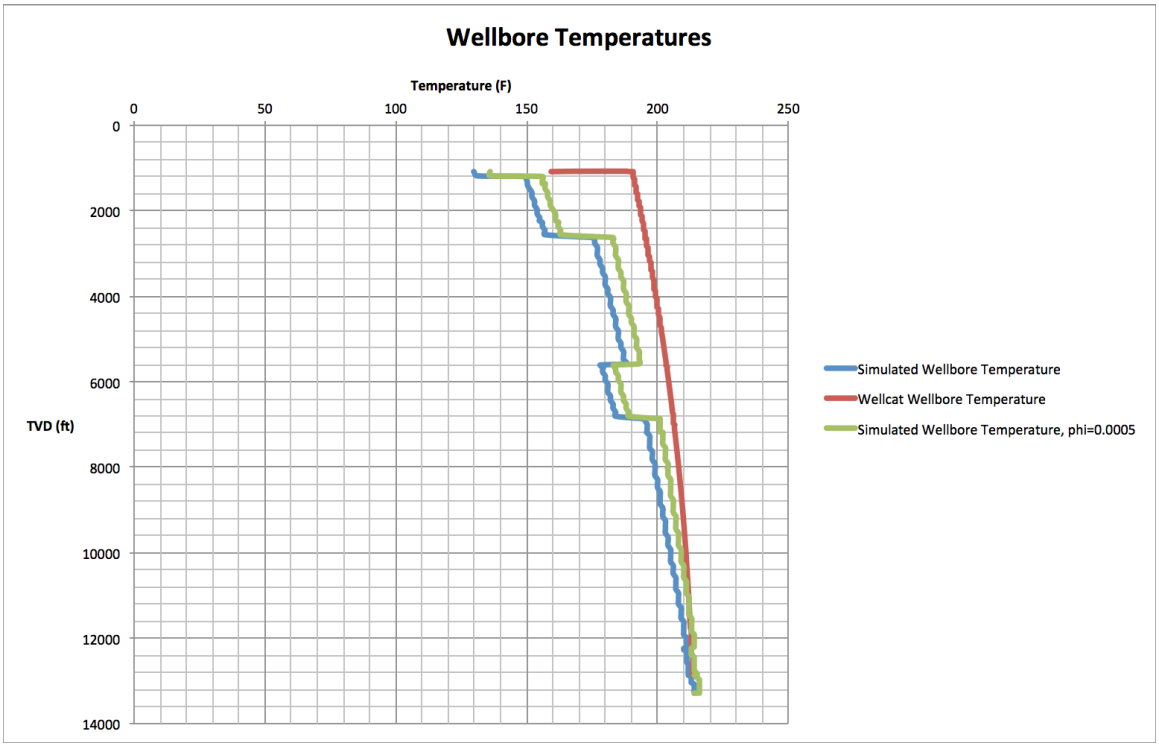

Figure 5-7 Wellbore Temperatures with Effect of ϕ

Figure 5-7 shows the simulated wellbore temperature in blue and the WellCat wellbore temperature in red plotted against true vertical depth. The green plot shows the simulated wellbore temperature with ϕ=0.0005. The simulated results gave a higher difference in wellbore temperature where the annulus was cemented.

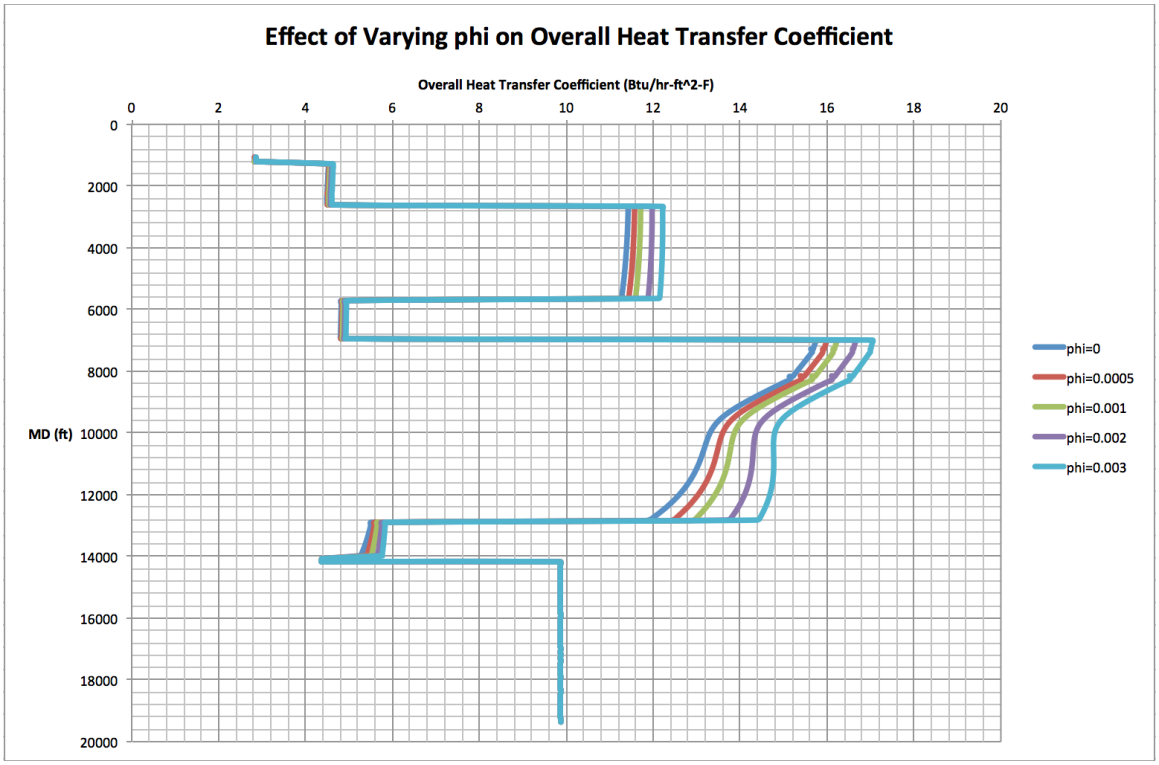

Figure 5-8 Effect of Varying ϕ on Overall Heat Transfer Coefficient

Figure 5-8 shows the effect of varying ϕ on the overall heat transfer coefficient. It can be seen that there was a difference at the areas not covered by cement below the surface casing shoe and below the intermediate casing shoe. The coefficient was increasing for increasing values of ϕ.

5.3.4 Time Effect

The following three figures show the difference in simulated fluid temperature in red and WellCat simulated temperature in blue. Figure 5-9 shows the difference with production time set to one hour, Figure 5-10 shows the difference with production time set to 10 000 hours and Figure 5-11 shows the difference with production time set to 200 000 hours.

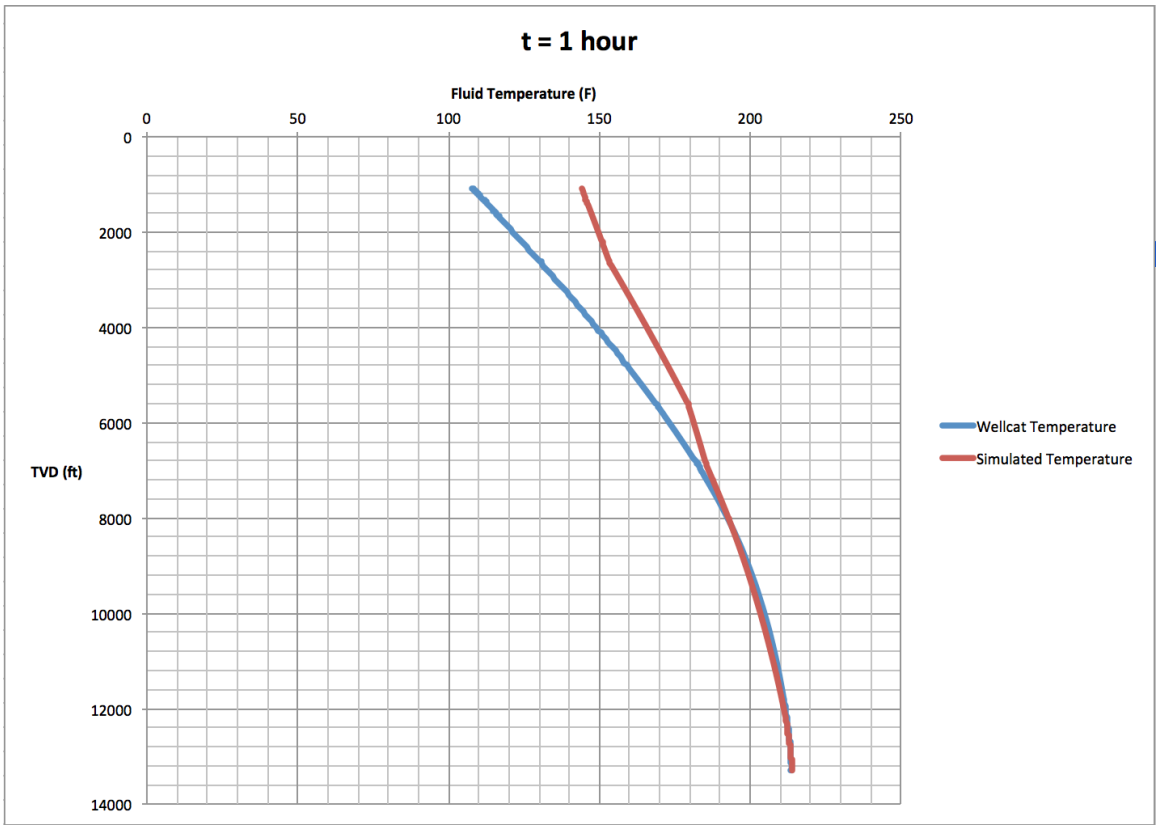

Figure 5-9 Fluid Temperatures, t=1 hour

Figure 5-10 Fluid Temperatures, t=10 000 hours

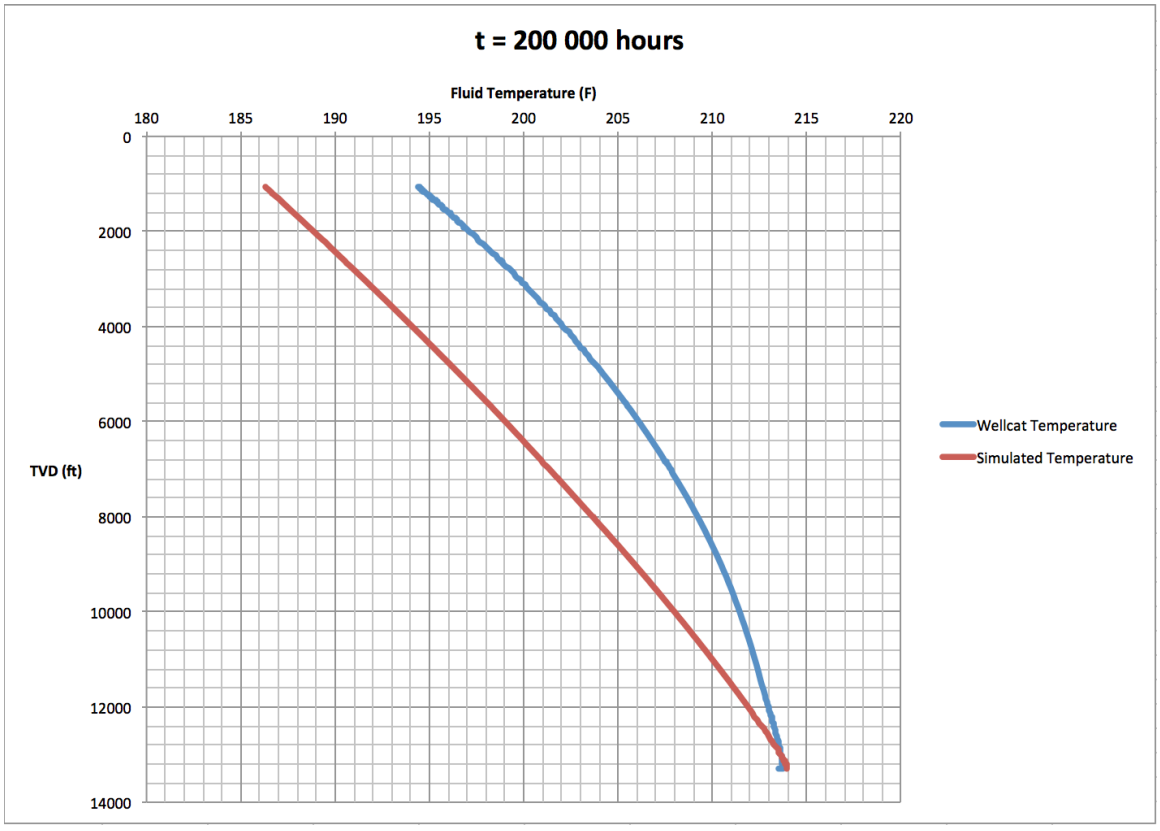

Figure 5-11 Fluid Temperatures, t=200 000 hours

For the production time set to one hour the simulated fluid temperature was above the WellCat temperature, while the simulated fluid temperature was below the WellCat temperature for the two higher production times.

5.3.5 Neglecting Convection

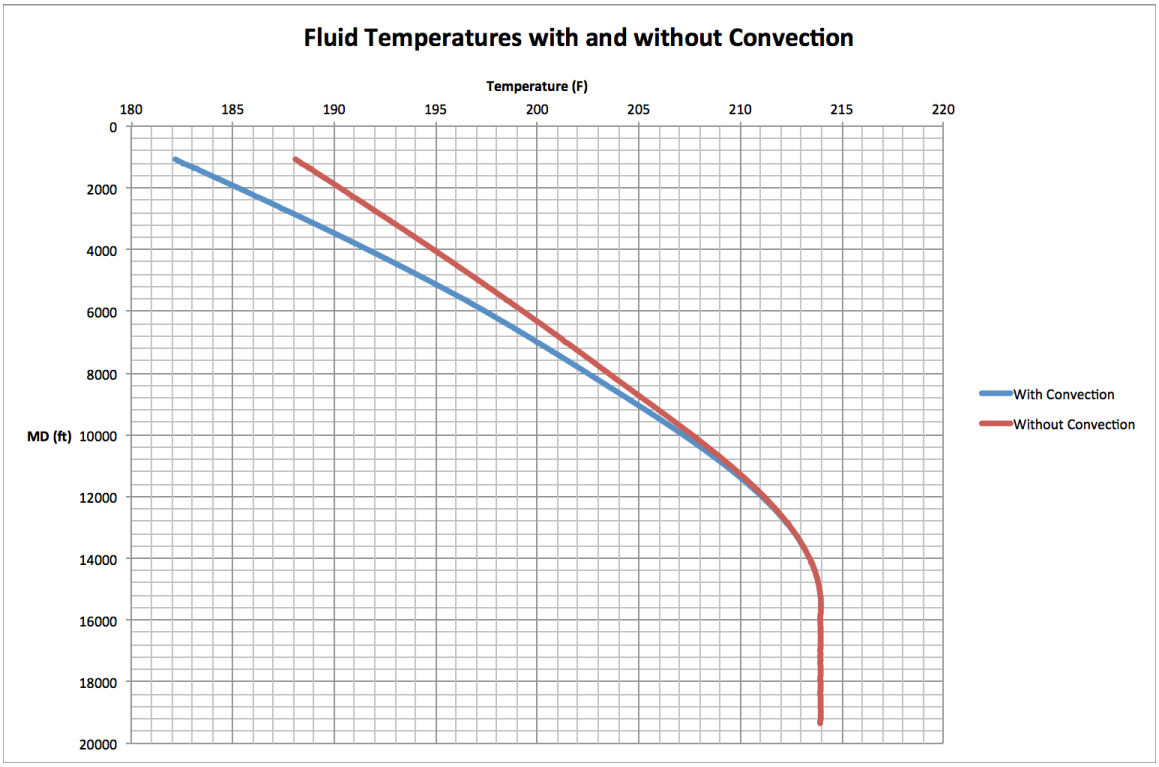

Figure 5-12 Fluid Temperatures with and without Convection

Figure 5-12 shows the fluid temperature with convection in blue and the fluid temperature without convection in red.

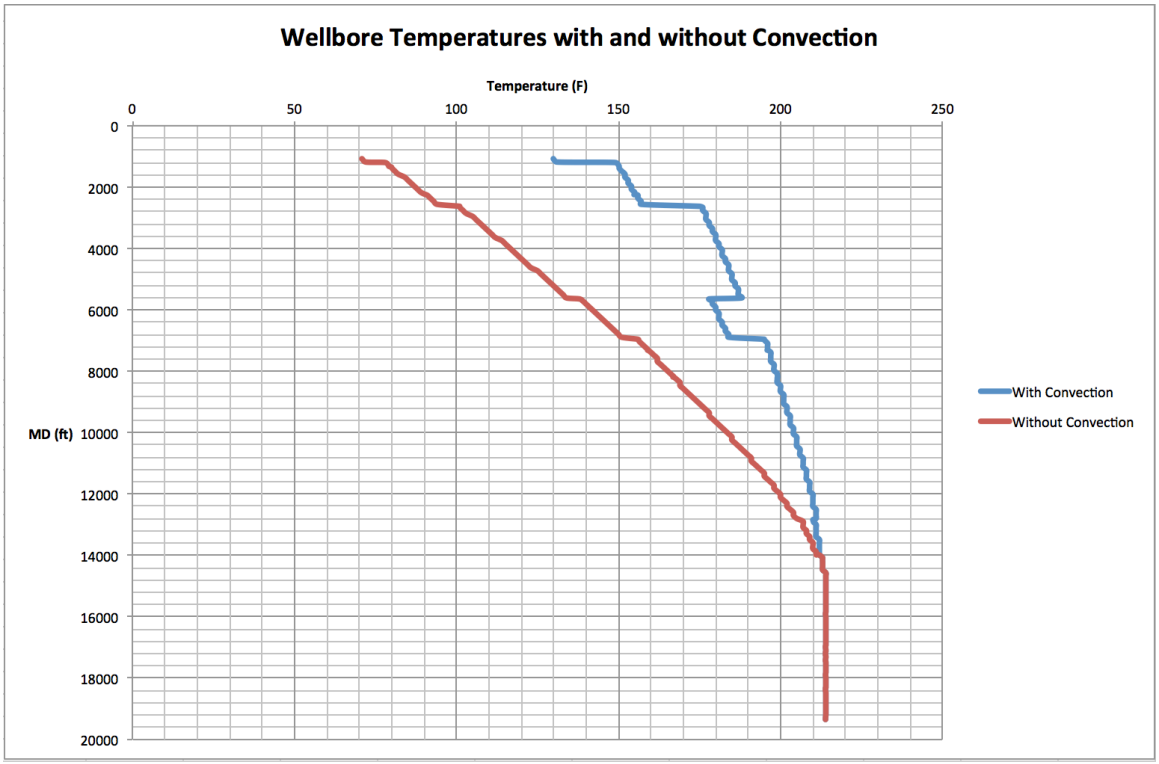

Figure 5-13 Wellbore Temperatures with and without Convection

Figure 5-13 shows the wellbore temperature with convection in blue and the wellbore temperature without convection in red.

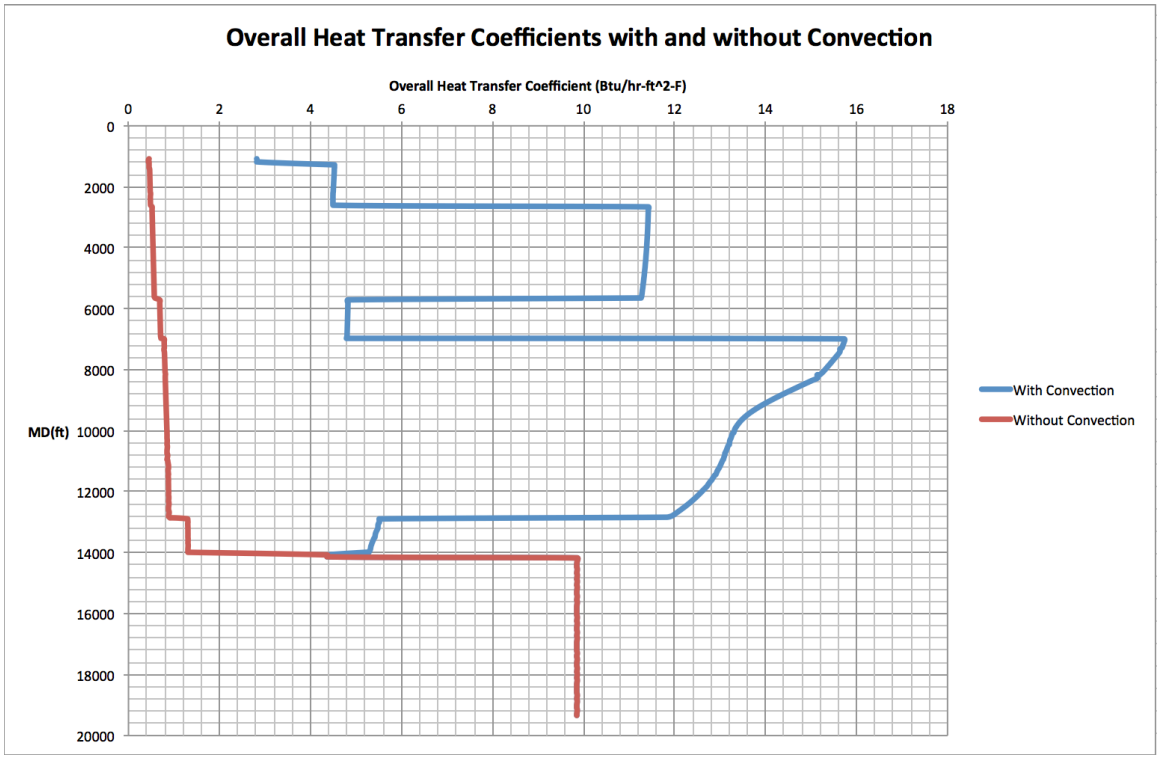

Figure 5-14 Overall Heat Transfer Coefficients with and without Convection

Figure 5-14 shows the overall heat transfer coefficient with convection in blue and the overall heat transfer coefficient without convection in red.

5.3.6 Neglecting Radiation

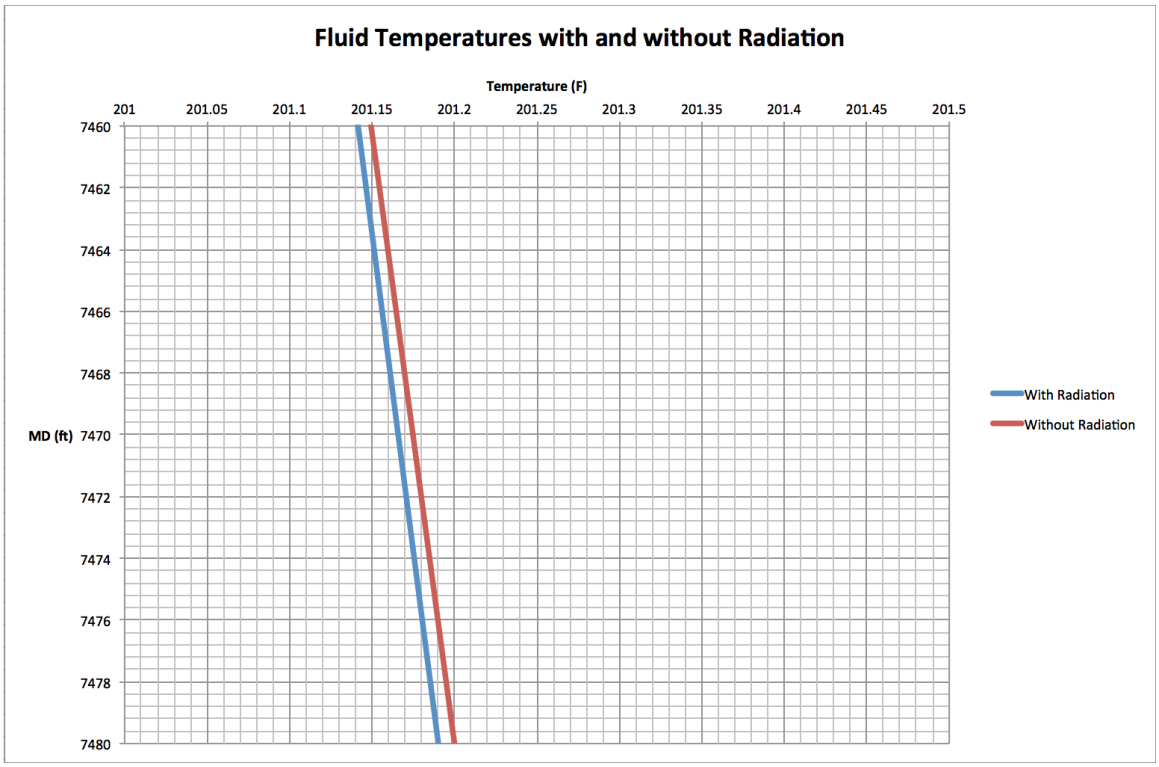

Figure 5-15 Fluid Temperatures with and without Radiation

Figure 5-15 shows a zoomed in area on the plot of the fluid temperature with radiation in blue and the fluid temperature without radiation in red. The temperature axis, i.e. the x-axis, on the plot has a difference in minimum and maximum value of 0.5 degrees, and the measured depth axis, i.e. the y-axis, on the plot has a difference in minimum and maximum value of 20 feet. This was to highlight that there was very low difference in the fluid temperatures when neglecting radiation.

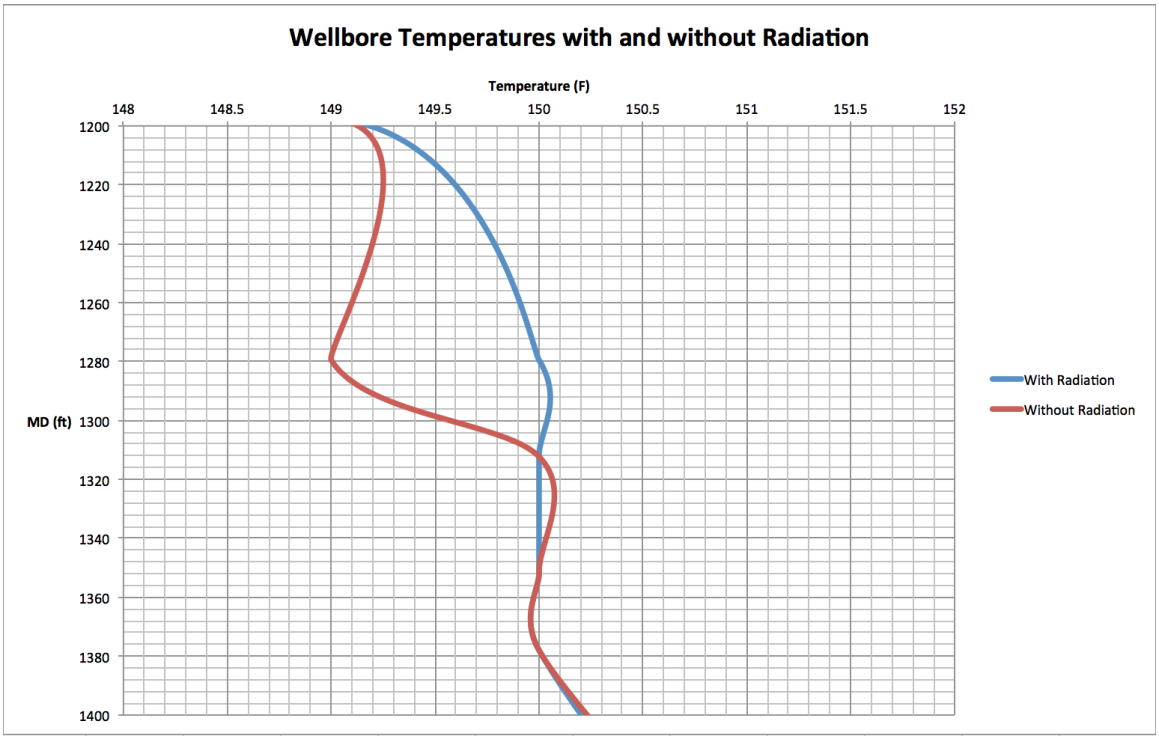

Figure 5-16 Wellbore Temperatures with and without Radiation

Figure 5-16 shows a zoomed in area on the plot of the wellbore fluid with radiation in blue and the wellbore temperature without radiation in red. The temperature axis, i.e. the x-axis, on the plot has a difference in minimum and maximum value of 4 degrees, and the measured depth axis, i.e. the y-axis, on the plot has a difference in minimum and maximum value of 200 feet.

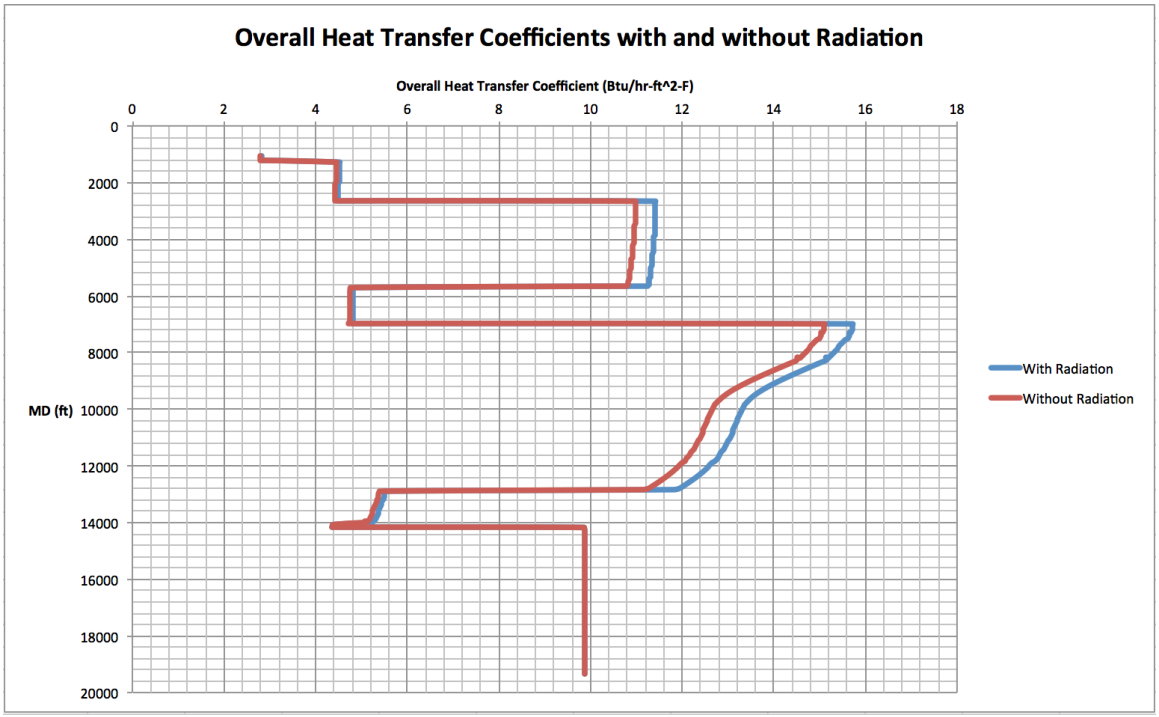

Figure 5-17 Overall Heat Transfer Coefficients with and without Radiation

Figure 5-17 shows the overall heat transfer coefficient with radiation in blue and the overall heat transfer coefficient without radiation in red.

More results can be found in Appendix C.

6 Discussion

The main purpose of this thesis was to establish a model for predicting the flowing fluid temperature based on existing literature and comparing with calculations from the ILS. The model was only compared to ILS results, no real data from existing wells or earlier models. Because of this, it is unclear if the ILS or the model gives the most correct temperatures in accordance with real data from existing wells.

6.1 Model Simulation

Figure 5-1 showed that the simulated temperature of the fluid had a discrepancy from the calculated fluid temperature in WellCat, with the fluid temperature being lower than the WellCat temperature. The same was the case for the wellbore temperatures. Figure 5-5 showed the difference in wellbore temperatures from the model and WellCat. WellCat seemed to be ignoring the decreases of wellbore temperature at the cemented areas of the well. This gave the wellbore temperatures on the cemented areas a higher value than what was modeled. This could also be an error in the model, but if it is the case that WellCat ignores the temperatures, the model might have more accurate results. Another reason that the WellCat temperature had higher values at these areas can be that there is a safety margin in WellCat

In Hasan and Kabir's paper from 1994 they did not use constant conductivity for the formation. In the simulation in this thesis it was assumed constant conductivity for the formation. The formation conductivity was used in the equations for wellbore temperature and the flowing fluid temperature. When changing the values for formation conductivity the fluid temperature increased for decreasing values of formation conductivity. This is shown in Figure 6-1.

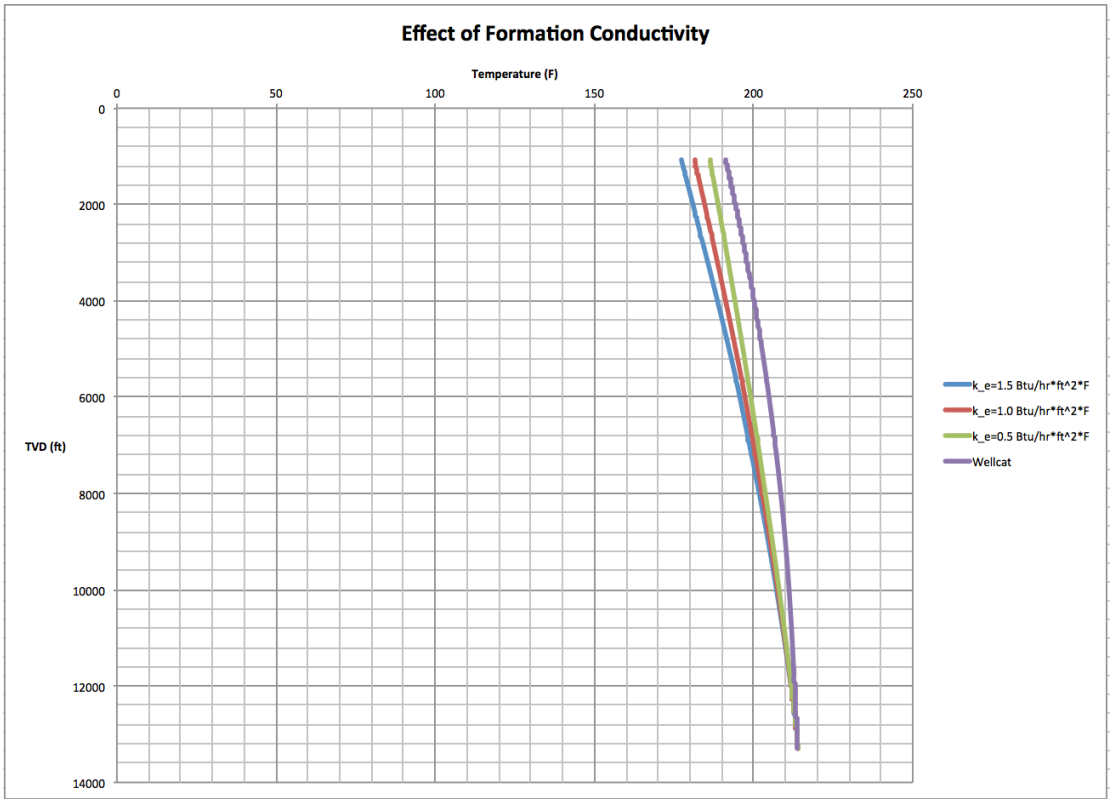

Figure 6-1 Effect of Formation Conductivity

6.2 Sensitivity of the Model

The sensitivity of the most important parameters was tested. These parameters were ϕ (correction factor including the Joule-Thomson effect used in the fluid temperature equation), β (thermal volumetric expansion coefficient of annulus fluid), time and heat transfer by convection and radiation in the annulus.

6.2.1 Sensitivity of ϕ

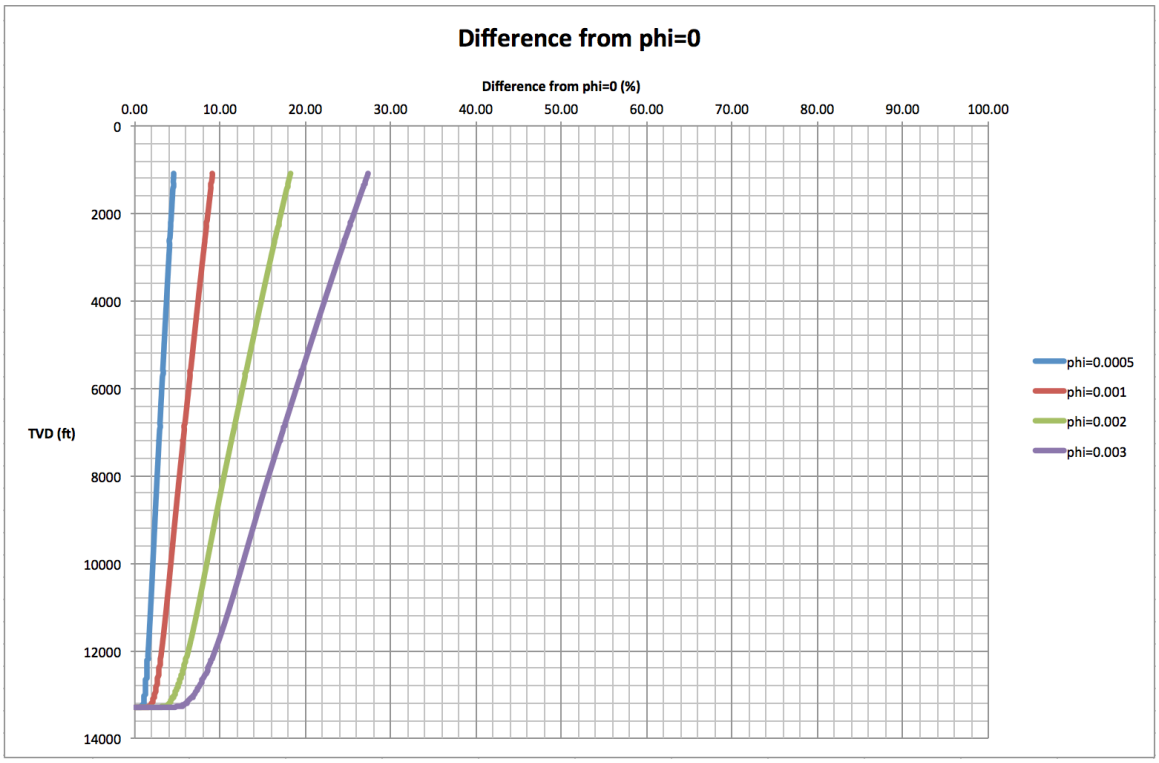

Figure 6-2 Fluid Temperature Difference for Varying ϕ

Figure 6-2 shows the difference in fluid temperature from ϕ=0, for ϕ=0.0005, ϕ=0.001, ϕ=0.002 and ϕ=0.003. The difference varied from 5% for ϕ=0 to 27% for ϕ=0.003.

From Figure 2-4 it is clear that when ϕ is changed, it affects the fluid temperature a lot. When using different values for ϕ, it could be seen that when ϕ=0.0005, the simulated result and the temperature obtained in WellCat were very close to each other. It could be seen that the values of ϕ had great importance with regards to getting the optimal result in comparison to WellCat results. ϕ=0.0005 also gave a value for the simulated wellbore temperature that was closer to the WellCat wellbore temperature.

WellCat does not give the equations that are used when calculating the fluid temperature. Therefore, it is hard to know what the source of error is. Since ϕ=0.0005 gave values close to the WellCat values, it is possible that one or more of the parameters in the equation of ϕ are the source of error. The expression for ϕ includes wellhead pressure, mass flow rate, GOR and specific gravities for oil and gas. For mass flow rate higher than 5 lbm/sec ϕ is assumed to be zero (Sagar et al., 1991).

From equation (22) it is clear that when the specific gravities for oil and gas is increased, ϕ increases. The same is the case when the wellhead pressure and the mass flow rate increases. When the GOR or the geothermal gradient is increased, ϕ decreases. Since increasing values of ϕ give increased temperatures, increasing the specific gravities for oil and gas, wellhead pressure or mass flow rate, increases the fluid and wellbore temperatures in the well. Increasing the GOR or the geothermal gradient decreases the fluid and wellbore temperatures in the well.

Figure 6-2 shows that the highest difference between ϕ=0 and ϕ=0.0005 was 5% and the highest difference between ϕ=0 and ϕ=0.003 was 27%.

6.2.2 Sensitivity of Time

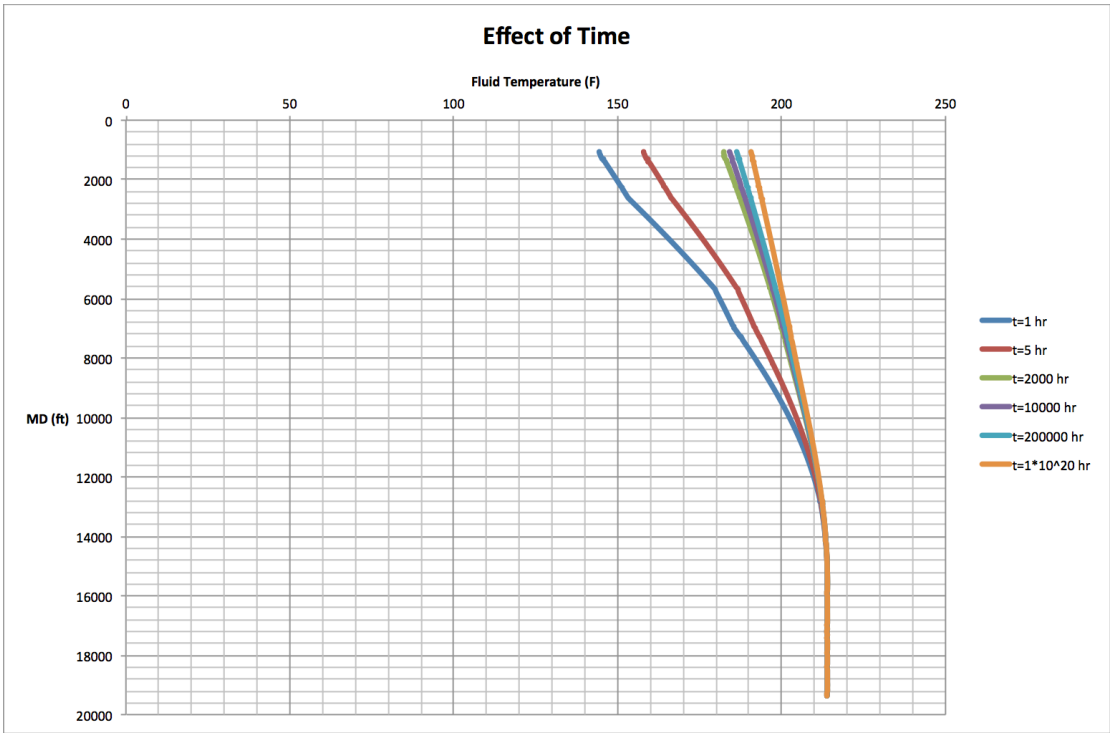

Figure 6-3 Effect of Time

Figure 6-3 shows the effect of time on the fluid temperature. The simulated production times to enlighten the effect were t=1 hour, t=5 hours, t=2 000 hours, t=10 000 hours, t=200 000 hours and $t=1\times10^{20}$ hours. The dark blue line shows the fluid temperature for t=1 hour.

For a short production time, 1 hour, the simulation gave a higher temperature than WellCat. At longer production times the opposite happened. One reason for this could be that the temperature prediction is less stable for short production times. This is

highlighted in Figure 6-3, where the temperatures at longer production times are close to each other, whereas the temperatures at 1 hour and 5 hours are far from each other.

Time is used in one equation in the model, i.e. equation (46), which gives the dimensionless time. For the short production times, here tested at 1 hour and 5 hours, the dimensionless time was below 1.5 for all wellbore radii. Therefore, the dimensionless temperature was calculated with a different equation for shorter production times than for longer production times. The two different equations are equations (52) and (53).

6.2.3 Sensitivity of Convection and Radiation

When neglecting the convection from the annulus there was high difference in the overall heat transfer coefficients for the entire well, except from the part with no annulus. This was expected, because convection is not used where there is no annulus. Because of the high difference in the overall heat transfer coefficient, the fluid temperature and the wellbore temperature also showed high differences.

Neglecting the radiation lead to small differences in both fluid temperature and wellbore temperature, while some differences were found at the sections with no cement. Zooming in on the temperature plots highlighted the small differences.

Comparing the results that were found when neglecting convection and radiation, it could be seen that it had much greater effect when neglecting the convection than when neglecting the radiation. This is because the heat transfer coefficient for convection is greater than the heat transfer coefficient for radiation. Since the overall heat transfer coefficient includes parts that include the convection and radiation coefficients in the denominator, it becomes smaller when neglecting convection than when neglecting radiation.

In the equations for heat transfer due to convection, the properties of the annulus fluids are used. All the properties of the annulus fluids are kept the same for A-, B- and C-annulus fluids in this model, except for the density. This gives an uncertainty for the results.

6.2.4 Sensitivity of β

β is the thermal volumetric expansion coefficient of annulus fluid. As equation (32) says, this equation is used for ideal gases. This equation was used for this model. If an ideal gas is not assumed equation (33) has to be used, where the annulus fluid density needs an iterative updating due to the annulus pressure. The effect of no ideal gas was not tested in this thesis.

6.3 Model Evaluation

As mentioned, the only comparisons that were made were between the model and the ILS. The assumptions that were made were conservative, which is an uncertainty for the model.

6.3.1 Model vs. ILS

WellCat does not show the calculations for the temperatures. It is likely that a safety margin is implemented in WellCat, which is not the case for the model. If a safety margin were assumed in WellCat, the temperature would be higher than the actual temperatures. Since there are no safety margins in the model that could be why the simulated temperatures were lower than the ILS temperatures.

6.3.2 Vertical Heat Transfer

Vertical heat transfer was not implemented in this model due to time restrictions. If this had been implemented it is assumed that it would have given some different results. For a vertical heat transfer model it is assumed that the heat transfer of the wellbore affects the formation temperature. Therefore, the formation temperature needs to be updated for a specified number of grids in a user-specified distance away from the wellbore.

7 Conclusion

The most important findings of this thesis were:

- A model for flowing fluid temperature prediction was established in Matlab.
- The effect of ϕ was tested, and a value of 0.005 gave flowing fluid temperatures that were very close to WellCat flowing fluid temperatures.
- The effect of neglecting convection and radiation was tested. Neglecting convection gave a high discrepancy in the results, while neglecting radiation gave a low discrepancy.
- The effect of changing production times was tested, where the temperature differences between the model and WellCat stabilized with higher production times.
- Due to conservative assumptions and little insight to the WellCat calculations, the model had some uncertainty.

8 Further Work

Due to time restrictions, the model was not perfected. Some further work has to be done for that to happen. Some of the changes that can be done are the following:

- Implement vertical heat transfer in the model.
- Modification of the model to work for transient flow.
- Updating of annulus density due to the thermal volumetric expansion coefficient of annulus fluid.
- Compare results to real data from existing wells.

9 Nomenclature

A = Area (m^2)

A = Heat flow area (ft^2)

A = Inverse relaxation distance (ft)

A_i = Inside area (in^2)

A_o = Outside area (in^2)

A_x = Area (in^2)

C = Compressibility of the fluid (psi^{-1})

C = Integration constant

c_{an} = Annulus fluid heat capacity (Btu/lb-°F)

c_e = Formation heat capacity (Btu/lb-°F)

C_J = Joule-Thomson coefficient (dimensionless)

c_{pm} = Wellbore fluid heat capacity (Btu/lbm-°F)

C_T = Coefficient of thermal expansion ($°F^{-1}$)

C_T = Thermal storage parameter

D = Diameter of inside completion string (ft)

$\frac{dQ_{in}}{dz}$ = Rate of heat coming in (Btu/hr)

$\frac{dQ_{out}}{dz}$ = Rate of heat coming out (Btu/hr)

$\frac{dT}{dx}$ = Temperature gradient (K/m)

E = Young's modulus (psi)

F = Force (lbf)

F_b = Axial tensile force (lb)

F_F = Force due to frictional drag (lb)

F_p = Axial force (lb)

F_T = Force due to temperature change (lb)

F_{tci} = View factor (dimensionless)

g = Acceleration due to gravity (=4.17×10^8 ft/hr^2)

g = Gravity acceleration (ft/sec^2)

g_c = Conversion factor (=32.2 lbm-ft/lbf-sec^2)

g_G = Geothermal gradient (°F/ft)

Gr = Grashof number (dimensionless)

g_T = Geothermal temperature gradient (°F/ft)

H = Fluid enthalpy (Btu/lbm)

h_c = Convective heat transfer coefficient (Btu/hr-ft^2-°F)

h_c = Convective heat transfer coefficient for fluid in annulus (Btu/°F-hr-ft^2)

$h_{c,A}$ = Convection heat transfer coefficient for A-annulus (Btu/hr-ft^2-°F)

$h_{c,B}$ = Convection heat transfer coefficient for B-annulus (Btu/hr-ft^2-°F)

$h_{c,C}$ = Convection heat transfer coefficient for C-annulus (Btu/hr-ft^2-°F)

h_r = Radiation heat transfer coefficient (W/m^2-K)

h_r = Radiative heat transfer coefficient (Btu/hr-ft^2-°F)

h_r = Radiative heat transfer coefficient for annulus (Btu/°F-hr-ft^2)

$h_{r,A}$ = Radiation heat transfer coefficient for A-annulus (Btu/hr-ft^2-°F)

$h_{r,B}$ = Radiation heat transfer coefficient for B-annulus (Btu/hr-ft^2-°F)

$h_{r,C}$ = Radiation heat transfer coefficient for C-annulus (Btu/hr-ft^2-°F)

$i\max$ = Number of grids around the wellbore

k = Thermal conductivity (W/m-K)

k_{cas} = Casing material conductivity (Btu/hr-ft-°F)

k_{cem} = Cement conductivity (Btu/hr-ft-°F)

k_e = Earth conductivity (Btu/hr-ft-°F)

k_{ha} = Thermal conductivity of annular fluids (Btu/hr-ft-°F)

k_{hc} = Equivalent thermal conductivity of annular fluids (Btu/hr-ft-°F)

k_{ins} = Insulation material conductivity (Btu/hr-ft-°F)

k_t = Tubing material conductivity (Btu/hr-ft-°F)

k_{tub} = Tubing material conductivity (Btu/hr-ft-°F)

L = Length of tubing (ft)

P = Annulus pressure (psi)

p = Pressure (psi)

$p_{hydrostatic}$ = Hydrostatic pressure (psi)

Pr = Prandtl number (dimensionless)

p_{wh} = Wellhead pressure (psi)

$q^{"}$ = Convective heat transfer (W/m^2)

Q = Heat flow rate (Btu/hr)

Q = Heat transfer per unit length (Btu/hr)

Q_c = Annulus heat flow due to natural convection and conduction (Btu/hr)

Q_{cas} = Heat flow casing (Btu/hr)

Q_{cem} = Heat flow cement (Btu/hr)

Q_r = Annulus heat flow due to radiation (Btu/hr)

q_{rad} = Radiation heat transfer (W/m^2)

$q_x^{"}$ = Conductive heat transfer rate in x-direction (W/m^2)

r = Radial distance from wellbore (ft)

r_{ci} = Casing inside radius (ft)

$r_{ci,9}$ = Inside radius of the $9^{5/8}$" casing (ft)

$r_{ci,13}$ = Inside radius of the $13^{3/8}$" casing (ft)

$r_{ci,20}$ = Inside radius of the 20" casing (ft)

$r_{ci,30}$ = Inside radius of the 30" casing (ft)

r_{co} = Casing outside radius (ft)

$r_{co,9}$ = Outside radius of the $9^{5/8}$" casing (ft)

$r_{co,13}$ = Outside radius of the $13^{3/8}$" casing (ft)

$r_{co,20}$ = Outside radius of the 20" casing (ft)

$r_{co,30}$ = Outside radius of the 30" casing (ft)

r_D = Dimensionless radius

r_e = Maximum distance from wellbore to formation

R_{gL} = °Gas/liquid ratio (scf/STB)

r_h = Drill hole radius (ft)

r_{ins} = Insulation surface radius (ft)

r_{ti} = Tubing inside radius (ft)

r_{to} = Tubing outside radius (ft)

r_{wb} = Wellbore or cement outside radius (ft)

$r_{wb,7}$ = Radius for wellbore drilled before the 7" section (ft)

$r_{wb,9}$ = Radius for wellbore drilled before the $9^{5/8}$" section (ft)

$r_{wb,13}$ = Radius for wellbore drilled before the $13^{3/8}$" section (ft)

$r_{wb,20}$ = Radius for wellbore drilled before the 20" section (ft)

$r_{wb,30}$ = Radius for wellbore drilled before the 30" section (ft)

T_{∞} = Fluid temperature (K)

T = Temperature (°F)

t = Time (sec)

T_{an}^{*} = Average temperature of the fluid in the annulus (°R)

T_{ci} = Casing inside temperature at surface (°F)

T_{co} = Outside casing temperature (°F)

T_D = Dimensionless temperature

t_D = Dimensionless time

T_{ebh} = Bottomhole formation temperature (°F)

T_{ei} = Undisturbed formation temperature at any given depth (°F)

T_{eibh} = Undisturbed bottomhole formation temperature (°F)

T_f = Tubing fluid temperature (°F)

T_{fbh} = Bottomhole fluid temperature (°F)

T_g = Temperature of formation away from wellbore (°F)

T_h = Cement-formation interface temperature (°F)

T_s = Surface temperature (K)

T_{sur} = Surroundings temperature (K)

T_{to} = Tubing outside temperature at surface (°F)

TVD = True vertical depth (ft)

T_w = Inside tubing temperature (°F)

T_{wb} = Interface temperature wellbore/earth (°F)

U = Overall heat transfer coefficient (Btu/hr-ft^2-°F)

U_{to} = Overall heat transfer coefficient (Btu/hr-ft^2-°F)

v = Specific volume (ft^3/lbm)

W = Total mass flow rate (lbm/sec)

w_t = Total mass flow rate (lbm/sec)

z = Depth from surface (ft)

z_{bh} = Total depth from surface (ft)

α = Coefficient of thermal expansion of annular fluid ($°F^{-1}$)

α = Formation heat diffusivity (ft^2/hr)

β = Thermal volumetric expansion coefficient of annulus fluid ($°R^{-1}$)

γ_{API} = Oil gravity (°API)

γ_g = Gas specific gravity

$\frac{\Delta L}{L}$ = Fractional length change

ΔL = Length increment of tubing or casing (ft)

ΔL_{bal} = Length change due to ballooning (ft)

ΔL_F = Length change due to frictional drag (ft)

ΔL_T = Metal expansion (ft)

$\frac{\Delta p}{\Delta L}$ = Friction pressure drop (psi/ft)

Δp = Pressure increase due to thermal expansion (psi)

Δp_i = Applied internal pressure (psi)

Δp_o = Applied external pressure (psi)

ΔT = Average change in temperature from base case to load case (°F)

ΔT = Average temperature change in the annulus (°F)

ε = Emissivity (dimensionless)

ε = Strain (dimensionless)

ε_{ci} = Casing inside emissivity at surface (dimensionless)

ε_{to} = Tubing outside emissivity at surface (dimensionless)

θ = Pipe inclination angle from horizontal (Degrees)

μ = Poisson's ratio (dimensionless)

μ_{an} = Annulus fluid viscosity (lbm/ft-hr)

ρ = Fluid density (psi/ft)

ρ_{an} = Annulus fluid density (lb/ft^3)

ρ_e = Density (lbm/ft^3)

σ = Stefan-Boltzmann constant (=5.67×10^{-8} W/m^2-K^4)

σ = Stephan-Boltzmann constant (=1.713×10^{-9} ft^2-hr-R^4)

σ = Stress (psi)

ϕ = Correction factor including the Joule-Thomson effect for each length interval in the well (dimensionless)

10 References

BELLARBY, J. 2009. *Well Completion Design,* Amsterdam, Amsterdam : Elsevier Science.

BERGMAN, T. L., DEWITT, D. P., INCROPERA, F. P. & LAVINE, A. S. 2011. *Fundamentals of heat and mass transfer,* New York, Wiley.

DROPKIN, D. & SOMERSCALES, E. 1965. Heat Transfer by Natural Convection in Liquids Confined by Two Parallel Plates Which Are Inclined at Various Angles With Respect to the Horizontal. *ASME,* 10.1115/1.3689057.

HASAN, A. R. & KABIR, C. S. 1991. Heat Transfer During Two-Phase Flow in Wellbores; Part I--Formation Temperature. Society of Petroleum Engineers.

HASAN, A. R. & KABIR, C. S. 1994. Aspects of Wellbore Heat Transfer During Two-Phase Flow (includes associated papers 30226 and 30970).

HASAN, A. R., KABIR, C. S. & WANG, X. 2009. A Robust Steady-State Model for Flowing-Fluid Temperature in Complex Wells.

IZGEC, B. 2008. *Transient Fluid and Heat Flow Modeling in Coupled Wellbore/Reservoir Systems.* PhD Dissertation, Texas A&M University.

LERVIK, Ø. 2015. Advanced Tubing Loads. NTNU: IPT.

LØBERGSLI, K. V. 2015. *Advanced Temperature Model for HPHT Conditions.* NTNU.

NORSOK D-010 2004. Well integrity in drilling and well operations. Standards Norway.

RAMEY, H. J., JR. 1962. Wellbore Heat Transmission.

SAGAR, R., DOTY, D. R. & SCHMIDT, Z. 1991. Predicting Temperature Profiles in a Flowing Well.

TØIEN, M. 2015. *Modell for casing design.* NTNU.

WILLHITE, G. P. 1967. Over-all Heat Transfer Coefficients in Steam And Hot Water Injection Wells.

Appendix A Tubing Stress Analysis

Stress and Strain of Tubing

One of the most important aspects of tubing stress analysis is to understand the behavior of metals under loads and the limits of what the metals can withstand. The loads on tubing come from a lot of different sources, e.g. pressure and temperature. It acts either axially, by compression or tension, or radially, by collapse or burst. A common term for it is stress (Bellarby, 2009):

$$\sigma = \frac{F}{A_x} \tag{71}$$

Where

σ = Stress (psi)

F = Force (lbf)

A_x = Area (in^2)

Stress will elongate the tubing. This elongation is given in the equation for strain, which is the fractional length change (Bellarby, 2009):

$$\varepsilon = \frac{\Delta L}{L} \tag{72}$$

Where

ε = Strain (dimensionless)

$\frac{\Delta L}{L}$ = Fractional length change

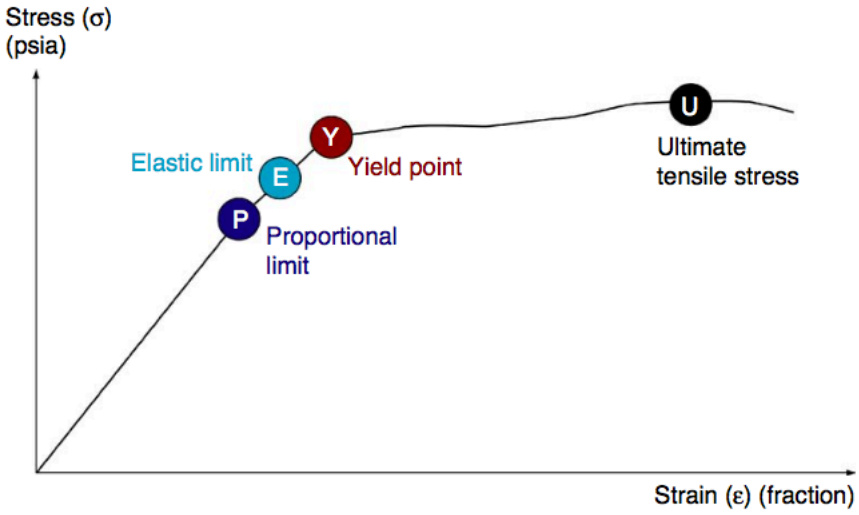

Figure A-1 Stress and Strain Relationship (Bellarby, 2009)

Stress and strain has a linear relationship until the yield point is reached. This linear relationship is the basis for Hooke's law, which gives the modulus of elasticity or Young's modulus, i.e. the slope of the linear line (Bellarby, 2009):

$$E = \frac{\sigma}{\varepsilon} \tag{73}$$

Where

E = Young's modulus (psi)

The elastic limit shows the point where the non-permanent deformation, i.e. elastic deformation, ends, and the permanent, i.e. plastic deformation, starts. The elastic limit lies close to the yield point, where there begins to be a large increase in strain, for a small increase in stress. This makes it difficult to measure it accurately. The API yield stress is defined as the minimum strength of the grade of the pipe, and it lies above the yield point (Bellarby, 2009).

Temperature has an effect on the strength of materials, especially for alloys, but also for carbon steel. Heating processes are often used to improve the properties of the steel, but it can also result in a reduction in yield stress. If this happens downhole and the temperatures are too high, it can lead to creep of the material (Bellarby, 2009).

Axial Loads

Axial loads are loads that occur along the length of the tubing. They can be either tensile or compressive forces (Bellarby, 2009).

Weight of Tubing

The load that is acting on the tubing initially, when the tubing is hanging free, is the weight hanging below. This means that at the bottom of the tubing there are no loads acting on it, while at the top there is the worst case, with the full weight of the entire tubing transferred to either the hanger or slips (Bellarby, 2009).

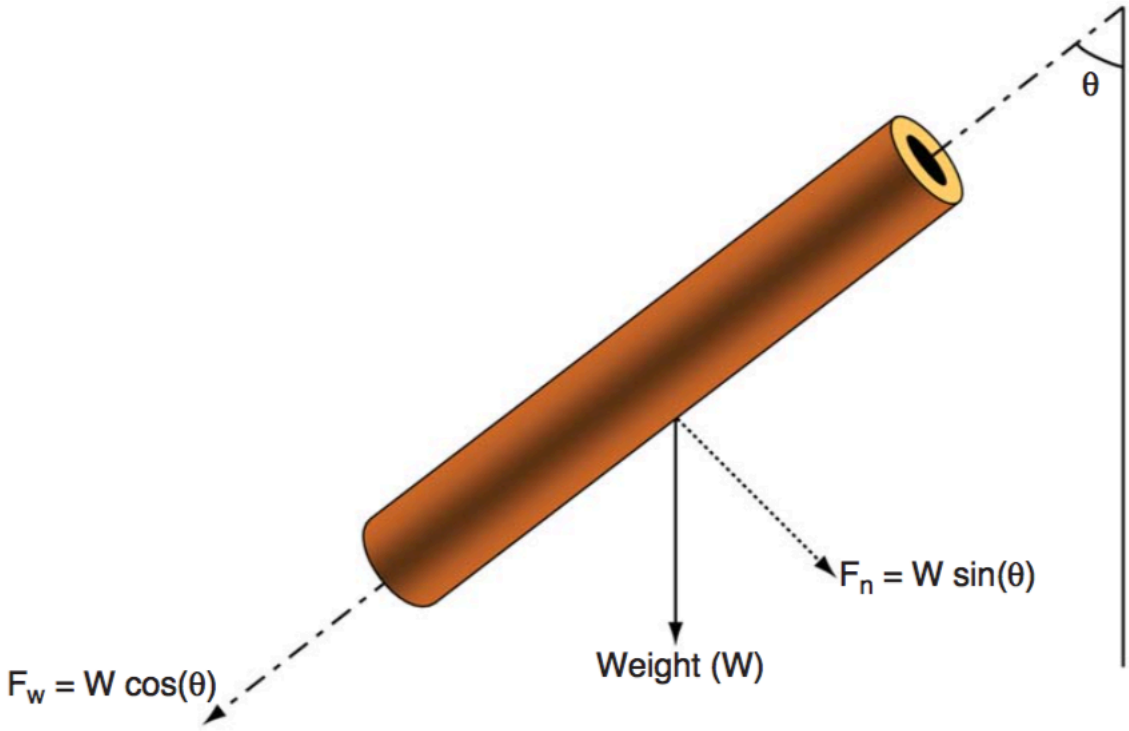

Figure A-2 Weight of Tubing (Bellarby, 2009)

Buoyancy

Buoyancy is a piston force, i.e. a load caused directly by pressure on cross-sections of pipe that are exposed. It occurs when tubing that is free to move has applied pressure to the base (Figure A-3) (Bellarby, 2009).

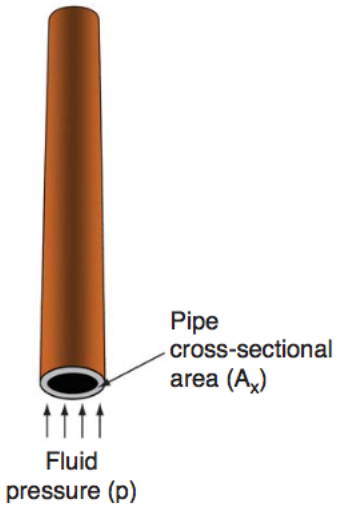

Figure A-3 Piston Forces (Bellarby, 2009)

An axial force is generated by the pressure applied, a compressional force when pressure is applied underneath the tubing. This force is given by (Bellarby, 2009):

$$F_p = -pA_x \tag{74}$$

Where

F_p = Axial force (lb)

p = Pressure (psi)

The pressure can come from both applied pressure and hydrostatic pressure.

$$p_{hydrostatic} = \rho * TVD \tag{75}$$

Where

$p_{hydrostatic}$ = Hydrostatic pressure (psi)

ρ = Fluid density (psi/ft)

TVD = True vertical depth (ft)

Ballooning

A tube loaded in axial tension generates axial and radial compressive strain. These two types of strain are proportional to each other in the elastic region. The following equation relates them to each other (Bellarby, 2009):

$$\mu = -\frac{Radial\ Strain}{Axial\ Strain} \quad \textbf{(76)}$$

Where

μ = Poisson's ratio (dimensionless)

(Eq.) is called Poisson's ratio and is the material property. It is slightly temperature dependent. This relationship is also applicable for axial compression, except that radial expansion occurs. This radial strain effect that comes from either axial tension or compression is often called the ballooning effect in tubulars (Bellarby, 2009). When pressure is applied to tubing, ballooning occurs. If it is fixed tubing, an axial tensile force is generated. This tensile force is generated from applied internal pressure and axial compression from applied external pressure. The force is given by the following equation (Bellarby, 2009):

$$F_b = 2\mu(A_i \Delta p_i - A_o \Delta p_o) \quad \textbf{(77)}$$

Where

F_b = Axial tensile force (lb)

A_i = Inside area (in^2)

Δp_i = Applied internal pressure (psi)

A_o = Outside area (in^2)

Δp_o = Applied external pressure (psi)

If the tubing is free to move, the applied internal pressure will shrink the tubing, while the applied external pressure will elongate the tubing. This occurs by applying Hooke's law (Bellarby, 2009):

$$\Delta L_{bal} = \frac{-2\mu L}{E(A_o - A_i)}(\Delta p_i A_i - \Delta p_o A_o) \quad \textbf{(78)}$$

Where

ΔL_{bal} = Length change due to ballooning (ft)

L = Length of tubing (ft)

The pressure changes described will in addition cause either an inward or an outward movement of the tubing, which will displace or compress fluid on the other side of the tubing (Bellarby, 2009).

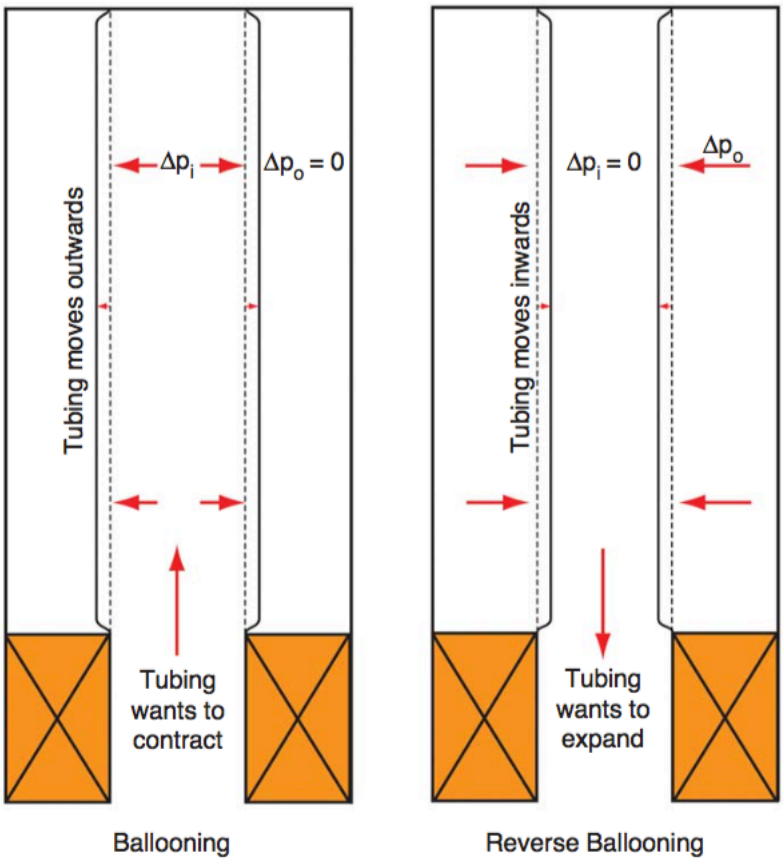

Figure A-4 Ballooning and Reverse Ballooning (Bellarby, 2009)

Appendix B Overall Heat Transfer Coefficients

Step 1 Overall Heat Transfer Coefficient

The iteration needs to start from the bottom, with the production liner. The variable that is changing in this section is the overall heat transfer coefficient. The entire production liner is cemented, so the following is the equation for U_{to}:

$$U_{to} = \left[\frac{r_{to} \ln \frac{r_{to}}{r_{ti}}}{k_{tub}} + \frac{r_{to} \ln \frac{r_{wb,7}}{r_{to}}}{k_{cem}} \right]^{-1} \quad \textbf{(79)}$$

Where

$r_{wb,7}$ = Radius for wellbore drilled before the 7" section (ft)

k_{tub} = Tubing material conductivity (Btu/hr-ft-°F)

Step 2 Overall Heat Transfer Coefficient

Since the top of cement for the production liner exceeds the shoe of the production casing, the first overall heat transfer coefficient for this section includes both heat transfer for the radius of the liner and the casing. The short interval where there is two cement interfaces, gives the following expression for U_{to}:

$$U_{to} = \left[\frac{r_{to} \ln \frac{r_{to}}{r_{ti}}}{k_{tub}} + \frac{r_{to} \ln \frac{r_{ci,9}}{r_{to}}}{k_{cem}} + \frac{r_{to} \ln \frac{r_{co,9}}{r_{ci,9}}}{k_{cas}} + \frac{r_{to} \ln \frac{r_{wb,9}}{r_{co,9}}}{k_{cem}} \right]^{-1} \quad \textbf{(80)}$$

Where

$r_{ci,9}$ = Inside radius of the $9^{5/8}$" casing (ft)

$r_{co,9}$ = Outside radius of the $9^{5/8}$" casing (ft)

$r_{wb,9}$ = Radius for wellbore drilled before the $9^{5/8}$" section (ft)

Step 3 Overall Heat Transfer Coefficient

This section includes A-annulus instead of cement between the tubing and the production casing. Therefore, the equation for U_{to} becomes:

$$U_{to} = \left[\frac{r_{to} \ln \frac{r_{to}}{r_{ti}}}{k_{tub}} + \frac{1}{h_{c,A} + h_{r,A}} + \frac{r_{to} \ln \frac{r_{co,9}}{r_{ci,9}}}{k_{cas}} + \frac{r_{to} \ln \frac{r_{wb,9}}{r_{co,9}}}{k_{cem}} \right]^{-1} \quad \textbf{(81)}$$

Where

$h_{c,A}$ = Convection heat transfer coefficient for A-annulus (Btu/hr-ft^2-°F)

$h_{r,A}$ = Radiation heat transfer coefficient for A-annulus (Btu/hr-ft^2-°F)

Step 4 Overall Heat Transfer Coefficient

This section consists of A-annulus and B-annulus, so U_{to} becomes:

$$U_{to} = \left[\frac{r_{to} \ln \frac{r_{to}}{r_{ti}}}{k_{tub}} + \frac{1}{h_{c,A} + h_{r,A}} + \frac{r_{to} \ln \frac{r_{co,9}}{r_{ci,9}}}{k_{cas}} + \frac{r_{to}}{r_{co,9}\left(h_{c,B} + h_{r,B}\right)} \right]^{-1} \quad \textbf{(82)}$$

Where

$h_{c,B}$ = Convection heat transfer coefficient for B-annulus (Btu/hr-ft^2-°F)

$h_{r,B}$ = Radiation heat transfer coefficient for B-annulus (Btu/hr-ft^2-°F)

Step 5 Overall Heat Transfer Coefficient

This section includes A-annulus, B-annulus and cement. U_{to} is given as:

$$U_{to} = \left[\frac{r_{to} \ln \frac{r_{to}}{r_{ti}}}{k_{tub}} + \frac{1}{h_{c,A} + h_{r,A}} + \frac{r_{to} \ln \frac{r_{co,9}}{r_{ci,9}}}{k_{cas}} + \frac{r_{to}}{r_{co,9}\left(h_{c,B} + h_{r,B}\right)} + \frac{r_{to} \ln \frac{r_{co,13}}{r_{ci,13}}}{k_{cas}} + \frac{r_{to} \ln \frac{r_{wb,13}}{r_{co,13}}}{k_{cem}} \right]^{-1} \quad \textbf{(83)}$$

Where

$r_{ci,13}$ = Inside radius of the $13^{3/8}$" casing (ft)

$r_{co,13}$ = Outside radius of the $13^{3/8}$" casing (ft)

$r_{wb,13}$ = Radius for wellbore drilled before the $13^{3/8}$" section (ft)

Step 6 Overall Heat Transfer Coefficient

This section includes A-annulus, B-annulus and C-annulus and U_{to} is given as:

$$U_{to} = \left[\frac{r_{to} \ln \frac{r_{to}}{r_{ti}}}{k_{tub}} + \frac{1}{h_{c,A} + h_{r,A}} + \frac{r_{to} \ln \frac{r_{co,9}}{r_{ci,9}}}{k_{cas}} + \frac{r_{to}}{r_{co,9}\left(h_{c,B} + h_{r,B}\right)} + \frac{r_{to} \ln \frac{r_{co,13}}{r_{ci,13}}}{k_{cas}} + \frac{r_{to}}{r_{co,13}\left(h_{c,C} + h_{r,C}\right)} \right]^{-1}$$

(84)

Where

$h_{c,C}$ = Convection heat transfer coefficient for C-annulus (Btu/hr-ft^2-°F)

$h_{r,C}$ = Radiation heat transfer coefficient for C-annulus (Btu/hr-ft^2-°F)

Step 7 Overall Heat Transfer Coefficient

The surface casing section has a constant equation for U_{to}, since it is cemented all the way to the top, with three annuli:

$$U_{to} = \left[\frac{r_{to} \ln \frac{r_{to}}{r_{ti}}}{k_{tub}} + \frac{1}{h_{c,A} + h_{r,A}} + \frac{r_{to} \ln \frac{r_{co,9}}{r_{ci,9}}}{k_{cas}} + \frac{r_{to}}{r_{co,9}\left(h_{c,B} + h_{r,B}\right)} + \frac{r_{to} \ln \frac{r_{co,13}}{r_{ci,13}}}{k_{cas}} + \frac{r_{to}}{r_{co,13}\left(h_{c,C} + h_{r,B}\right)} + \frac{r_{to} \ln \frac{r_{co,20}}{r_{ci,20}}}{k_{cas}} + \frac{r_{to} \ln \frac{r_{wb,20}}{r_{co,20}}}{k_{cem}} \right]^{-1}$$

(85)

Where

$r_{ci,20}$ = Inside radius of the 20" casing (ft)

$r_{co,20}$ = Outside radius of the 20" casing (ft)

$r_{wb,20}$ = Radius for wellbore drilled before the 20" section (ft)

Step 8 Overall Heat Transfer Coefficient

As for the surface casing section the conductor casing section has a constant equation for U_{to}, and in addition to three annuli, it is cemented outside both the surface casing and the conductor. Therefore, the equation becomes:

$$U_{to} = \left[\frac{r_{to} \ln \frac{r_{to}}{r_{ti}}}{k_{tub}} + \frac{1}{h_{c,A} + h_{r,A}} + \frac{r_{to} \ln \frac{r_{co,9}}{r_{ci,9}}}{k_{cas}} + \frac{r_{to}}{r_{co,9}\left(h_{c,B} + h_{r,B}\right)} + \frac{r_{to} \ln \frac{r_{co,13}}{r_{ci,13}}}{k_{cas}} + \frac{r_{to}}{r_{co,13}\left(h_{c,C} + h_{r,C}\right)} + \frac{r_{to} \ln \frac{r_{co,20}}{r_{ci,20}}}{k_{cas}} + \frac{r_{to} \ln \frac{r_{ci,30}}{r_{co,20}}}{k_{cem}} + \frac{r_{to} \ln \frac{r_{co,30}}{r_{ci,30}}}{k_{cas}} + \frac{r_{to} \ln \frac{r_{wb,30}}{r_{co,30}}}{k_{cem}} \right]^{-1}$$

(86)

Where

$r_{ci,30}$ = Inside radius of the 30" casing (ft)

$r_{co,30}$ = Outside radius of the 30" casing (ft)

$r_{wb,30}$ = Radius for wellbore drilled before the 30" section (ft)

Appendix C Additional Results

Production Rate

The production flowing rate was changed to investigate its effect on the model. The flow rate of 3 lbm/sec where included, but may give a faulty result due to ϕ=0 only for values over 5 lbm/sec. The production rates that were investigated were 3 lbm/sec, 15 lbm/sec, 35 lbm/sec, 70 lbm/sec, 140 lbm/sec and 300 lbm/sec.

Figure C-1 shows the different fluid temperatures for the various production rates.

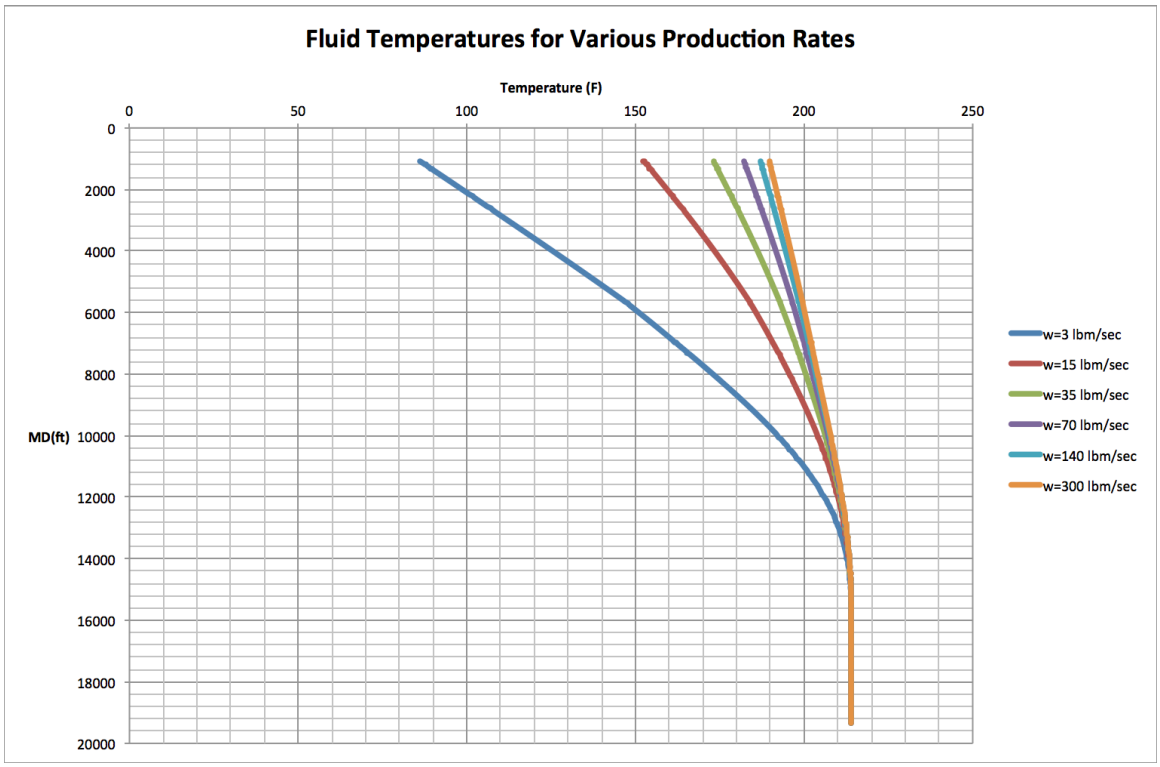

Figure C-1 Fluid Temperatures for Various Production Rates

Figure C-2 shows the different wellbore temperatures for the various production rates.

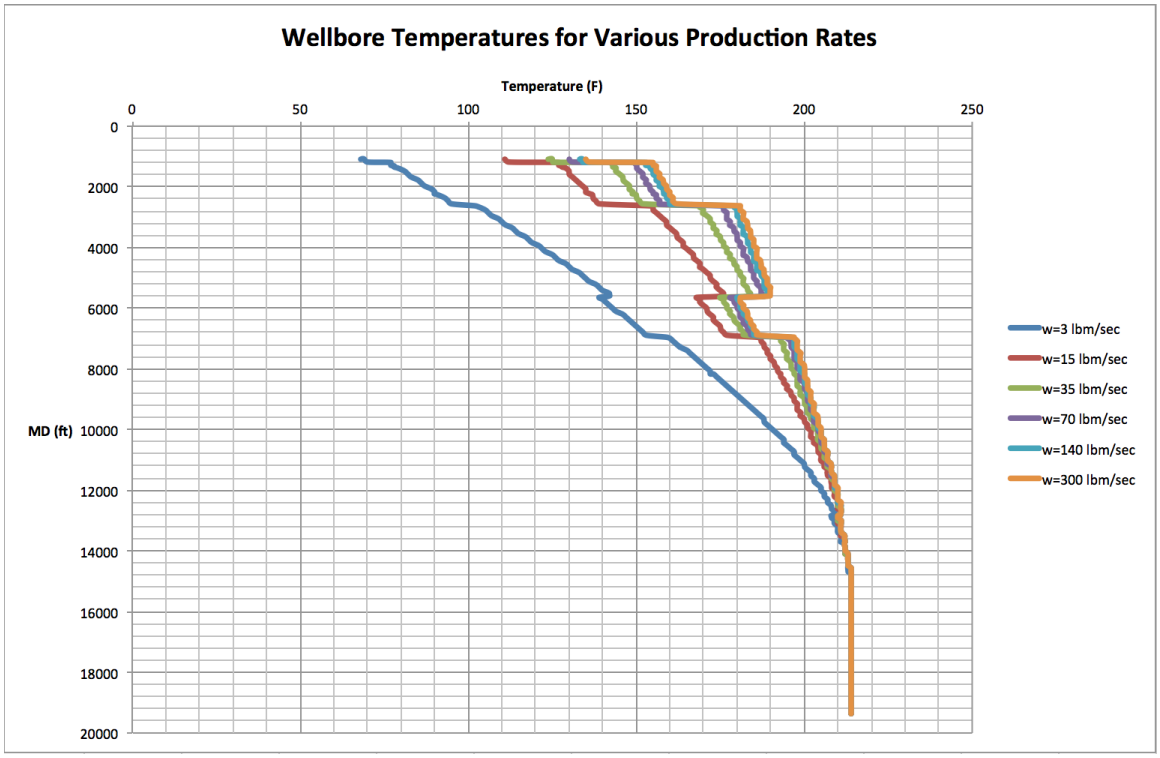

Figure C-2 Wellbore Temperatures for Various Production Rates

Figure C-3 shows the different overall heat transfer coefficients for the various production rates.

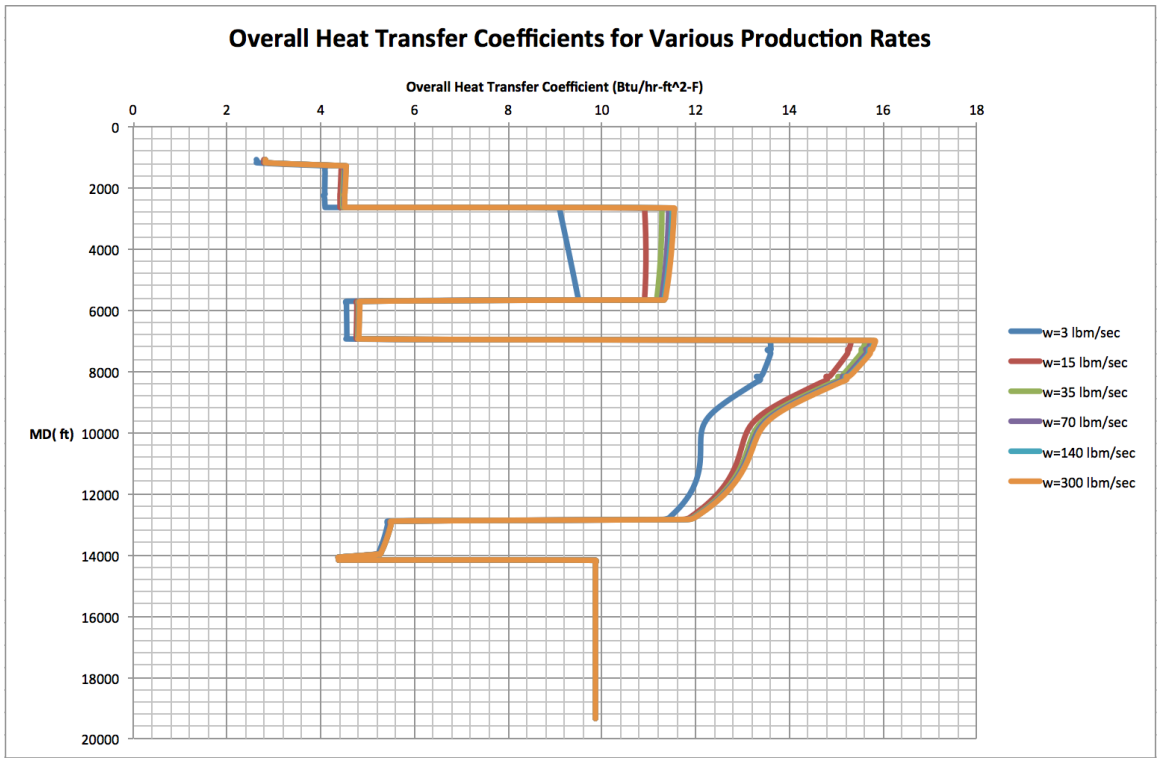

Figure C-3 Overall Heat Transfer Coefficients for Various Production Rates